EBioMedicine 39 (2019) 315–331

Contents lists available at ScienceDirect

EBioMedicine

journal homepage: www.ebiomedicine.com

EBioMedicine
Published by THE LANCET

Zika virus induces strong inflammatory responses and impairs homeostasis and function of the human retinal pigment epithelium

Yannick Simonin [a,1], Nejla Erkilic [b,1], Krishna Damodar [b], Marion Clé [a], Caroline Desmetz [c], Karine Bolloré [a], Mehdi Taleb [a], Simona Torriano [b], Jonathan Barthelemy [a], Grégor Dubois [b], Anne Dominique Lajoix [c], Vincent Foulongne [d], Edouard Tuaillon [d], Philippe Van de Perre [d], Vasiliki Kalatzis [b,*,2], Sara Salinas [a,*,2]

[a] Pathogenesis and Control of Chronic Infections, INSERM, Etablissement Français du Sang, University of Montpellier, Montpellier, France
[b] Institute for Neurosciences of Montpellier, INSERM, University of Montpellier, Montpellier, France
[c] BioCommunication en CardioMétabolique, University of Montpellier, Montpellier, France
[d] Pathogenesis and Control of Chronic Infections. INSERM, University of Montpellier, Etablissement Français du Sang, CHU Montpellier, Montpellier, France

ARTICLE INFO

Article history:
Received 8 October 2018
Received in revised form 19 November 2018
Accepted 6 December 2018
Available online 20 December 2018

ABSTRACT

Background: Zika virus (ZIKV) has recently re-emerged as a pathogenic agent with epidemic capacities as was well illustrated in South America. Because of the extent of this health crisis, a number of more serious symptoms have become associated with ZIKV infection than what was initially described. In particular, neuronal and ocular disorders have been characterized, both in infants and in adults. Notably, the macula and the retina can be strongly affected by ZIKV, possibly by a direct effect of the virus. This is supported by the detection of replicative and infectious virus in lachrimal fluid in human patients and mouse models.
Methods: Here, we used an innovative, state-of-the-art iPSC-derived human retinal pigment epithelium (RPE) model to study ZIKV retinal impairment.
Findings: We showed that the human RPE is highly susceptible to ZIKV infection and that a ZIKV African strain was more virulent and led to a more potent epithelium disruption and stronger anti-viral response than an Asian strain, suggesting lineage differences. Moreover, ZIKV infection led to impaired membrane dynamics involved in endocytosis, organelle biogenesis and potentially secretion, key mechanisms of RPE homeostasis and function.
Interpretation: Taken together, our results suggest that ZIKV has a highly efficient ocular tropism, which creates a strong inflammatory environment that could have acute or chronic adverse effects.
Fund: This work was funded by Retina France, REACTing and La Région Languedoc-Roussillon.

1. Introduction

Zika virus (ZIKV) is a small single-stranded RNA enveloped arbovirus, member of the *Flaviviridae* family that was first isolated in Uganda in 1947 [1]. Two lineages exist, namely African and Asian, the latter of which resulted from its emergence in Southeast Asia, where it caused local limited outbreaks. After reaching Southeast Asia, the virus further spread throughout the Pacific islands, causing a first proper epidemic in Yap in 2007, then in the French Polynesia in 2013, and lastly in South America in 2015 [2,3]. Most ZIKV-infected patients are asymptomatic, as is seen with other arboviral infections. When symptoms are present, they usually consist of a maculopapular rash, febrile illness, cephalic pain, conjunctivitis and mild fever [4]. However, the extent of the South American epidemic brought to light additional severe pathologies in some patients. In particular, neurological symptoms, such as Guillain-Barré syndrome (GBS) and microcephaly (among other neurodevelopmental defects called congenital Zika syndrome, CZS), highlighted the potential neurovirulence of ZIKV and led the WHO to declare the epidemic a Public Health Emergency of International Concern. Other complications include thrombocytopenia as well as ophthalmological affections in microcephalic infants and in adults.

Similar to other arboviruses, the main transmission mode of ZIKV involves mosquito vectors, in particular *Aedes aegypti*. However, surprisingly, other modes of transmission have recently been described, including vertical, perinatal, sexual and potentially lacrimal transmissions [5,6]. This is due to the presence, sometimes for extended periods, of viral particles in body fluids, including blood [7], semen [8], vaginal secretions [9], urine [10], breast milk [11] and conjunctival fluid

* Corresponding authors.
E-mail addresses: vasiliki.kalatzis@inserm.fr (V. Kalatzis), sara.salinas@inserm.fr (S. Salinas).
[1] Equally contributed.
[2] Co-last authors.

https://doi.org/10.1016/j.ebiom.2018.12.010

Research in context

Evidence before this study

Zika virus (ZIKV) has recently re-emerged causing major epidemics, notably in Latin America. Phylogenetic analyses show the existence of one Asian and one African lineage. In addition to neurological anomalies, increasing reports of ocular anomalies in children and adults affected with the Asian strain have emerged, raising the possibility of direct viral targeting of the eye. Moreover, infectious ZIKV was detected in lachrymal liquid in human patients and mouse models, further suggesting a potential transmission route *via* the conjunctival fluid. However, very little was known regarding the molecular mechanisms of inflammation associated with ZIKV retinal infections and little is reported regarding the ocular pathogenesis associated with the ZIKV African strain.

Added value of this study

Here, we compared the virulence and pathogenesis of one African and one Asian ZIKV strain in the human retinal pigment epithelium (RPE) *in vitro*. We show that the African ZIKV strain had a higher infectivity and triggered stronger anti-viral and inflammatory response than the Asian strain. Furthermore, this led to more dramatic impairments of RPE architecture, homeostasis and function. Taken together, our results highlight the need to better characterize ZIKV ocular tropism and strain-dependent pathogenesis.

Implications of all the available evidence

The finding of an efficient ocular tropism and strong inflammatory responses associated with ZIKV infections may suggest that ocular defects, with short or long term effects, may be an important pathological trait of ZIKV. Consequently, these results may prompt clinicians to consider longitudinal follow up of patients who suffered from ophthalmological damages during the acute phase of infection.

[12,13]. The mechanisms of intrauterine and perinatal transmissions of ZIKV have recently been partially characterized. These studies have shown that ZIKV is capable of crossing the blood-placental barrier and highly infecting and replicating in the placenta and in developing fetal tissues, including the brain. This, in turn, is responsible for severe malformations at birth, which is illustrated by fetal demise and numerous cases of microcephaly and other CNS (central nervous system) impairments [14–16].

Although the eye is sequestered from the systemic circulation, numerous viruses can still reach this organ and cause inflammation and pathologies. Cytomegalovirus, as well as Ebola virus, are able to replicate efficiently in the eye, which has been consequently proposed to act as a viral reservoir [17–19]. Several arboviruses, including dengue virus (DENV), chikungunya virus (CHIKV) and West Nile virus (WNV), have been described to trigger ophthalmic damage, notably retinopathies [20–22]. In addition to important cortical defects, infants born with microcephaly displayed in many cases (~50–70%) ocular abnormalities such as chorioretinal impairment (including pigment molting of the retinal pigment epithelium; RPE) and optic nerve anomalies among others [23–26]. In adults, ZIKV infection can be found associated with conjunctivitis, uveitis [27], maculopathy [28,29] and chorioretinal lesions [17]. Inner retinal vasculopathy has also been described in a 38-year-old patient accompanied by irregularities and detachment of the RPE [30].

Ex vivo studies have shown that multiple cells of the retina can be targeted by ZIKV including retinal endothelial cells, pericytes, RPE and Müller cells [31–33]. In these cells, viral replication was associated with anti-viral responses and cytokine secretion, which could potentiate local inflammation and trigger lesions. In animal models, namely mice invalidated for the interferon (IFN) type I response (*Ifnar*$^{-/-}$) or young wild type (WT) mice, systemic ZIKV infection led to efficient targeting of the eye [32–35]. In these studies, retinal lesions were consistently found and the presence of ZIKV in various cell types of the retina confirmed. In ZIKV-infected mice, ophthalmological manifestations included conjunctivitis and panuveitis, accompanied by infection of the cornea, iris, optic nerve, and ganglion and bipolar neurons of the retina [35]. Moreover, shedding of viral RNA in tears of ZIKV-infected mice was also described and eye-derived ZIKV was found to be highly infectious [35].

The RPE, the supporting tissue of the retina, consists of a monolayer of epithelial cells that contributes to the retinal-blood barrier [36]. On its basal side, the RPE lies upon the Bruch's membrane, a collagenous layer separating it from the choriocapillaris. Epithelium integrity is dependent on lateral cell-cell contact, which requires efficient tight, adherens, and gap junctions [36]. On its apical side, microvilli are present and are in contact with the outer segments of photoreceptors. The RPE has many different roles including regulation of the visual cycle and the immune response in the eye [36,37]. RPE cells were proposed to serve as resident antigen presenting cells as they express HLA molecules at their cell surface [32,37,38]. Inflammatory responses in the RPE are often associated with pathologies, such as age-related macular degeneration (AMD).

The permissiveness of the RPE to viral infections makes it a pertinent tissue to study host-cell interactions [39–41]. RPE can be cultured *ex vivo* as a primary or a stem cell-derived tissue and still maintains its morphological and functional characteristics [42]. Furthermore, we [43] and others [44,45], have also shown that it can effectively differentiate from induced pluripotent stem cells (iPSC) and remain fully functional, thus providing access to large quantities of human tissue without ethical considerations. With this model of iPSC-derived RPE, we recently studied the effect of ZIKV infection on the human RPE and showed that ZIKV Asian lineage had a deleterious effect on its architecture [31]. Here, we further characterized ZIKV infection mechanisms in the retina by comparing the virulence and cellular effects, in particular the inflammatory responses, associated with ZIKV African and Asian strains in iPSC-derived human RPE, as differences in pathogenesis between the two lineages have been reported (reviewed in [46]). We show that ZIKV infection has major effects on RPE integrity and elicits a strong anti-viral response, as well as induction of several IFNs. Moreover, we show that basic functions of the RPE, such as phagocytosis and secretion are impacted by ZIKV infection.

2. Material and methods

2.1. Material

Antibodies used in this study are: mouse anti-pan-flavivirus (clone 4G2, MAB10216 Millipore), mouse anti-N-Cadherin (clone 5D5, Abcam), rabbit anti-ZO1 (#617300 Invitrogen), rabbit anti-β-catenin, (clone E247, Abcam), rabbit anti-MERTK antibody (#ab52968, Abcam), mouse anti-CRALBP, (#ab15051, Abcam), rabbit anti-GAPDH antibody (#G9545, Sigma-Aldrich), rabbit anti-Tyrosinase (#CSB-PA025394LA01HU, Cusabio Technology LTD), rabbit anti-PDI (#ab3672, Abcam).

2.2. Virus strains and cellular infections

H/PF/2013 ZIKV of Asian lineage (French Polynesia, 2013) and ArB41644 ZIKV of African lineage (Bangui, Central African Republic, 1989), isolated from mosquitoes by Pasteur Institute of Dakar were

produced and provided by the National Reference Center for arboviruses (NRC) at <5 passages on Vero cells [47]. Viral stocks were prepared by infecting sub confluent Vero cells at a multiplicity of infection (MOI) of 0.01 in DMEM medium (Thermoscientific) supplemented with 2% heat-inactivated fetal bovine serum (Sigma). Cell supernatant was collected 6 days later and viral stock harvested after centrifugation at 300*g* to remove cellular debris. Viral titers were determined by the 50% tissue culture infective dose (TCID50), which was calculated using the Spearman-Kärber method [48] and were expressed as TCID50 per mL.

2.3. IPSC-derived RPE generation and culture

Human iPSCs were generated from WT BJ fibroblasts (ATCC CRL2522) as previously described [49]. Briefly, to begin the spontaneous differentiation process, confluent iPSCs were cultured in Knockout DMEM medium (ThermoFischer Scientific) supplemented with 20% KO serum replacement (ThermoFischer Scientific), 1% GlutaMAX (ThermoFischer Scientific), 1% non-essential amino acids (ThermoFischer Scientific), 0.1% β-mercaptoethanol (ThermoFischer Scientific) and 1% penicillin-streptomycin (ThermoFischer Scientific). Approximately six weeks later, pigmented foci were manually dissected, pooled, dissociated with 0.25% trypsin, filtered through a 40-μm filter and seeded at a density of ~3×10^4 cells per 0.32 cm^2 on a 1/30 dilution Corning Matrigel HESC-qualified matrix (Dominique Dutscher). All analyses were performed on iPSC-derived RPE at P3.

2.4. Transepithelial resistance (TER) measurements

At P3, the iPSC-derived RPE was cultured on Matrigel-coated, clear BD Falcon cell culture inserts with high density 0.4 μM pores (Dominique Dutscher) in 24-well plates. The TER was measured using the Epithelial Volt/Ohm Meter EVOM2 (World Precision Instruments, Hertfordshire, U.K.) according to the manufacturer's instructions. Briefly, electrodes were sterilized in 70% ethanol for 5 min, rinsed and equilibrated in media, then placed in the compartmentalised chambers with the longer electrode vertically touching the bottom of the dish in the lower chamber and the shorter electrode in the upper chamber without touching the cell layer. TER was recorded once the value stabilised, approximately 5 s after placing the electrode. To calculate the final TER values (Ohms·cm^2), the background measurement of a Matrigel-coated insert without cells was subtracted from the reading and the value multiplied by the growth surface area.

2.5. Indirect immunofluorescence assays

IPSC-derived RPE plated on Matrigel-coated cell culture inserts was infected or mock-treated. For indirect IF, cells were fixed with 4% PFA and permeabilized with 0.1% Triton X-100/PBS for 5 min at room temperature (RT), followed by a blocking step with 2% bovine serum albumin (BSA) and 10% horse serum for 30 min to 1 h at RT. Primary and secondary antibodies were diluted in blocking solution and incubated sequentially for 1 h at RT. When indicated, cells were treated during the secondary antibody incubation with ActinGreen (ThermoFischer scientific). DAPI nuclei counter stain was performed during the secondary antibody incubation. Samples were mounted with fluorescent mounting medium (Mowiol) and imaged by confocal microscopy using the Zeiss SP85 confocal microscope, with 40× or 63 × 1.4 NA Plan Apochromat oil-immersion objectives.

2.6. Immunoblotting

IPSC-derived RPE grown in 24-well plates was scraped in cold PBS containing Complete protease inhibitor cocktail tablets (Roche) and centrifuged at 3000*g* for 5 min. The pellet was resuspended in 2× Laemmli's sample buffer (Biorad) containing 1/25 dilution of β-mercaptoethanol (Sigma-Aldrich) and Benzonase (Sigma-Aldrich). The samples were heated 5 min at 95 °C and loaded onto an AnyKD precast MiniProtean TGX Stain Free gel (Biorad). The separated proteins were electrotransferred using a Trans-Blot® Turbo™ PVDF Transfer Pack and System (Biorad). After blocking for 1 h in 0.5% Tween-PBS in 5% skim milk (blocking solution), membranes were incubated with 1:250 dilution of anti-ZO-1, 1:500, dilution of anti-N-Cadherin, 1:2000 dilution of anti-β-catenin, 1:2000 dilution of anti-MERTK, 1:1000 dilution of anti-CRALBP or with 1:1000 dilution of anti-GAPDH overnight at 4 °C. After 3 washes in 0.5% Tween-PBS, the membrane was incubated with 1:10,000 dilution of horseradish peroxidase (HRP)-conjugated sheep antibody against mouse (Jackson ImmunoResearch, Interchim, Montluçon), or goat antibody against rabbit (Sigma-Aldrich), whole immunoglobulins. The detection step was performed using the Amersham ECL prime western blotting detection reagent (GE Healthcare) and a Biorad Chemidoc XRS+ system.

2.7. RT-qPCR

IPSC-derived RPE grown in 24-well plates and infected with the two strains of ZIKV or mock-treated were harvested in RLT buffer (Qiagen). Total RNA was extracted using RNeasy® mini-kit (Qiagen). Complementary DNA was synthesized using Omniscript® reverse transcriptase (Life Technologies). RT^2 Profiler PCR arrays for Human Antiviral Response and for Human Interferons and receptors response (96 well format, Qiagen) were used for real-time quantitative PCR (RT-qPCR) analysis, with the LC480 real time PCR instrument (Roche) and the Light Cycler 480 SYBR Green I master Mix (Roche). Volumes of mix, cDNA, RNAse-free water, and cycling conditions were determined according to the manufacturer's instructions. Gene expression was normalized to that of the housekeeping gene *HPRT*. Genes without interpretable amplification curves were excluded from the analysis.

RT-qPCR on ZIKV-infected mouse eyes was performed as previously published [47]. Briefly, eyes were enucleated and tissue lysis performed with a Fastprep 24 apparatus (MP Biomedicals) and mRNA extraction with the Altona Diagnostics kit RealStar® Zika Virus RT-PCR Kit 1.0, according to the manufacturers' instructions. Cycle thresholds were converted to relative charges using ten-fold serial dilutions of a ZIKV culture supernatant extract. Experiments performed previously with similar MOI for ZIKV AF and AS showed equal amplification for both strains (data not shown).

2.8. Electron microscopy analyses

The cell culture inserts containing the iPSC-derived RPE were immersed in a solution of 2.5% glutaraldehyde in PHEM buffer (1×, pH 7.4) overnight at 4 °C. The inserts were then rinsed in PHEM buffer and post-fixed in a 0.5% osmic acid for 2 h in the dark at RT. After two rinses in PHEM buffer, the cells were dehydrated in a graded series of ethanol solutions (30–100%). The cells were embedded in EmBed 812 using an Automated Microwave Tissue Processor for Electronic Microscopy, Leica EM AMW. Semi-thin sections (700 nm) were stained with toluidine blue and observed under light microscopy. Thin sections (70 nm; Leica-Reichert Ultracut E) were counterstained with uranyl acetate 1.5% in 70% ethanol and lead citrate, and observed using a Tecnai F20 transmission electron microscope at 200 KV (CoMET, MRI facility, Montpellier).

2.9. Enzyme-linked immunosorbent assay (ELISA) and multiplex analyses

Proteins such as cytokines and survival factors were quantified in supernatants from Mock and ZIKV-infected RPE cells. Multiplexed microbead assays were used according to manufacturer's instructions (Merk Millipore). A first kit aiming to quantify CXCL10 was used in duplicate. Similar approach was undertaken with a second kit consisting of 5 cytokines: IFNα, IFNγ, IFNβ, IFNλ, IL2 and CXCL10. Readings were

performed on MAGPIX apparatus from Merck and data were analyzed using the xPONENT program. Mean concentrations (pg/ml) of cytokines were all superior to the detection limits, defined as the mean background value plus 2S.

Vascular endothelial growth factor (VEGF) and pigment epithelium-derived factor (PEDF) protein levels were measured by ELISA assays (R&D systems) according to the manufacturer's instructions. Readings were performed on a spectrophotometer (Thermofischer Scientifics).

2.10. POS internalization assay

Bovine neuroretinas were dissected, homogenized, placed in 20% sucrose and loaded onto a discontinuous sucrose gradient (20–60%). The gradient was ultracentrifuged at 75,600 xg for 1 h at 10 °C and the ROS, which sedimented in the 40% layer, were collected with a syringe, washed twice with HBSS (ThermoFischer Scientific), resuspended in 2.5% sucrose and stored at −80 °C. The concentration was estimated to 1.2×10^6 POS/μl by flow cytometry. Thawed ROS were washed twice in 0.1 M $NaHCO_3$, pH = 9, centrifuged 10 min at 21,130 xg at RT. The pellet was resuspended in 0.1 M $NaHCO_3$ containing 1:10 dilution of FITC Isomer I (Invitrogen Molecular Probes). The samples were kept in the dark overnight at 4 °C, then washed twice in PBS and resuspended in RPE media. RPE grown on cell culture inserts was incubated with 5 POS/cell for 2.5 h at 37 °C, then washed 5 times with cold PBS, fixed and permeabilized. The nuclei were then labeled with DAPI and the inserts mounted on glass slides with Mowiol (Sigma-Aldrich).

2.11. Mouse experiments and ethics statement

Pathogen-free *Ifnar*$^{-/-}$ mice [50] kindly provided by Dr. Gilles Uzé, were infected at E.C.E. (Etablissement Confiné d'Expérimentation), a level 3 animal facility of the University of Montpellier. Mice were bred and maintained according to the French Ministry of Agriculture and European institutional guidelines (Form A STE n°123). Experiments were performed according to national regulations and approved by the regional ethics committee of Languedoc-Roussillon (Comité Régional d'Ethique sur l'Expérimentation Animale- Languedoc-Roussillon), France (approval N° 6773-201609161356607).

Groups of 6 to 8 week-old mice were inoculated *via* an intraperitoneal route with 10^4 TCID50/ml of ZIKV AS or ZIKV AF. ZIKV-infected mice were euthanized at 7 dpi and eyes were collected after PBS intracardiac perfusion, fixed in 4% PFA and cut using a microtome (10 μm sections) at the RHEM facilities (Montpellier).

3. Results

3.1. African and Asian ZIKV lineages differentially infect RPE cells and impair cellular junctions and architecture

Numerous studies suggest differences in virulence between African and Asian ZIKV strains (ZIKV AF and ZIKV AS respectively) *in vitro* and *in vivo*, which could lead to differences in pathogenicity during human infection (reviewed in [46]). To determine whether the tropism observed previously with ZIKV AS in iPSC-derived human RPE [31] was also a feature of ZIKV AF, we infected RPE grown on cell culture inserts with a multiplicity of infection (MOI) of 0.1 with each strain and monitored viral production over a period of 4 days by the TCID50 method. Fig. 1A shows the kinetics of viral replication of ZIKV AF and AS and demonstrates a higher replication rate for ZIKV AF that could be observed from 48 h post-infection. This is similar to what we previously described in human neural stem cells (hNSCs) and human astrocytes [47]. This difference was maintained until 96 h post infection, where we observed a difference of ~1 log between the two strains (Fig. 1A). Because we previously showed that ZIKV AS infection led to an increase of epithelium permeability [31], we compared the transepithelial resistance (TER) of mock- (control, CT), ZIKV AF- and ZIKV AS-infected RPE at MOI 0.1 at 4, 7 and 11 days post-infection (dpi) (Fig. 1B). The maturation/impermeability of iPSC-derived RPE was demonstrated by the measured TER ranging around 300 Ohms·cm^2 (*in vivo*, RPE impermeability is characterized by a TER of 150 Ohms·cm^2 [51]). Interestingly, at 7 dpi, ZIKV AF rapidly led to a drop in TER whereas ZIKV AS did not yet have a flagrant effect. At 11 dpi however, both strains had dramatically decreased the TER (corresponding to a loss of impermeability (*i.e.* ≤20 Ohms·cm^2) of the RPE, compared to CT epithelia (Fig. 1B). Moreover, ZIKV AF and ZIKV AS were detected in the lower compartment at 4 dpi, when epithelium integrity was not yet affected, suggesting an efficient basal release, with a higher viral titer for ZIKV AF (Fig. 1C).

To monitor the epithelial organization/architecture after ZIKV infection, we performed indirect immunofluorescence (IF) studies on mock- and ZIKV-infected RPE grown on culture inserts (Fig. 1D and E). RPE cells mock-infected or infected with ZIKV AF or AS were fixed at 11 dpi and labeled to visualize actin and ZO-1 (a key protein of tight junctions, Fig. 1D) or β-catenin (a signaling protein also present in cellular junctions, Fig. 1E). Actin labeling showed dramatic epithelial reorganization in ZIKV AF-infected RPE cells, accompanied with destabilization/loss of the junction proteins ZO-1 and β-catenin (Fig. 1D and E), as compared to mock-infected cells. In ZIKV AS-infected RPE however, actin did not appear massively reorganized, and ZO-1 and β-catenin showed less drastic impairments compared to ZIKV AF-infected cells (Fig. 1D and E). We then used immunoblotting to monitor the protein expression of key actors in RPE signaling, organization and homeostasis. Mock- and ZIKV-infected RPE were lysed at 11 dpi. Consistent with the IF studies, immunoblot analyses showed that the adhesion/signaling proteins ZO-1, N-cadherin and β-catenin levels were significantly decreased ($p < .05$) in ZIKV AF-infected RPE, whereas ZIKV AS infection led to a significant decrease in only N-cadherin and β-catenin levels (Fig. 1F). The c-mer transmembrane tyrosine kinase receptor (MERTK), a major regulator of photoreceptor outer segment (POS) phagocytosis in RPE also showed significantly reduced levels ($p < .05$) in ZIKV AF- and ZIKV AS-infected cells, whereas the levels of the cellular retinaldehyde binding protein (CRALBP), an intracellular protein involved in the visual cycle, was only slightly, but significantly, decreased ($p < .05$) in ZIKV AF-infected cells (Fig. 1F).

To better visualize RPE architecture in mock- and ZIKV-infected conditions, we performed software-based 3D reconstruction of z-stacks from confocal images (Supplemental Fig. 1). Nuclei and actin rendering showed a good epithelial organization in mock-infected (CT) cells with well-defined cellular limits and basally located nuclei (Supplemental Fig. 1A). Similar to what we found by indirect IF, we detected a strong reorganization/impairment of actin and epithelial architecture in ZIKV AF-infected RPE, with nuclei sometimes mislocalized (Supplemental Fig. 1B). Epithelium organization seemed slightly perturbed in ZIKV AS-infected conditions, as the actin organization was less defined than in CT conditions (Supplemental Fig. 1C).

Taken together, these data suggest that ZIKV infection in RPE alter the expression and localization of adhesion proteins. Moreover, we found that ZIKV AF replicates more efficiently in RPE than ZIKV AS, and triggers more important changes in epithelial permeability and organization.

3.2. Ultrastructural changes in ZIKV-infected RPE cells

To confirm that ZIKV infection leads to important changes in epithelial organization, which could underlie the modulation in epithelial permeability, we performed electron microscopy studies in mock- and ZIKV-infected RPE at 10 dpi (Figs. 2 and 3). General epithelial organization was first monitored by staining of semi-thin sections (Fig. 2A). An intact and regular epithelial monolayer could be seen for the mock-infected (CT) epithelium. By contrast, ZIKV AF infection interrupted the integrity of the monolayer with holes present between cells. Following ZIKV AS infection, the monolayer appeared continuous but irregular and detached cells were detected on the apical side (Fig. 2A).

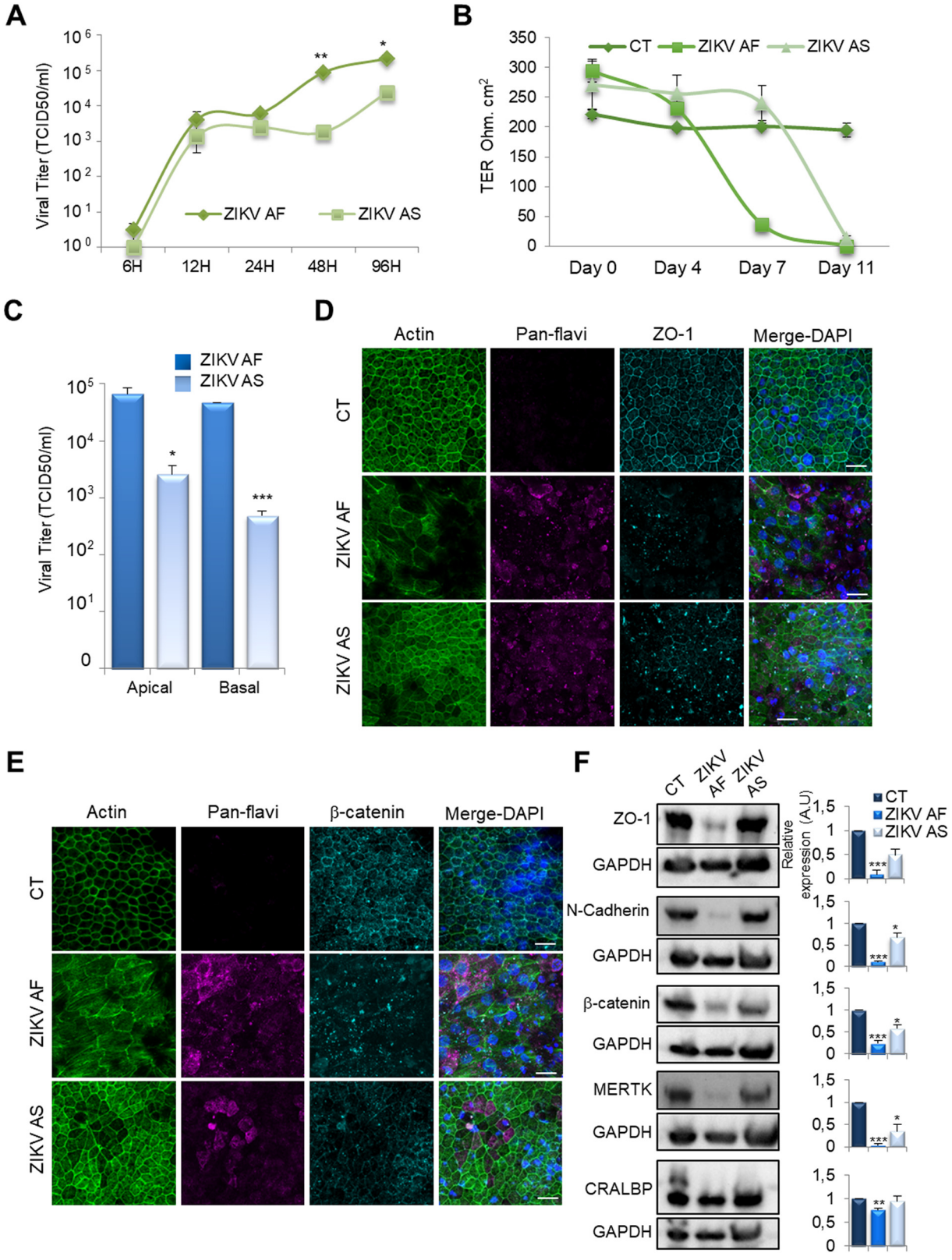

Fig. 1. ZIKV AF and ZIKV AS differentially infect and impair the RPE. IPSC-derived-RPE were infected with both ZIKV strains at MOI 0.1 over different time periods. (A) Viral titers in the supernatants of RPE grown in 96 well plates at various times post-infection were assayed by the TCID 50 method. Results are expressed as mean ± SEM of 3 independent experiments and each time point was compared between strains using an unpaired *t*-test, $^{*}p < .05$, $^{**}p < .01$. (B) Transepithelial resistance (TER) of mock (control, CT)- or ZIKV-infected RPE grown on cell culture inserts was measured at various dpi. Each point represents the mean ± SEM of 3 independent experiments. (C) Viral titers from apical and basal compartments of RPE grown on cell culture inserts at 4 dpi. Results are expressed as mean ± SEM of 3 independent experiments and analyzed using an unpaired *t*-test, $^{*}p < .05$, $^{***}p < .001$ (ZIKV AF compared to ZIKV AS). (D-E) Mock- and ZIKV-infected RPE grown on cell culture insert were fixed at 11 dpi. Indirect immunofluorescence studies were used to label actin (green), ZIKV (pan-flavi, magenta), ZO-1 (D, cyan) or β-catenin (E, cyan); as well as nuclei (DAPI, blue). Representative images of 2 independent experiments are shown. Scale bars 20 μm. (F) Western blot analysis of the expression of junction (ZO-1, N-Cadherin and β-catenin) and RPE (MERTK and CRALBP) markers in mock- and ZIKV-infected RPE at 11 dpi. Representative images are shown. The quantification of the expression of these markers, as a function of GAPDH expression, is expressed as means ± SEM of 3 experiments $^{*}p < .05$, $^{**}p < .01$, $^{***}p < .001$.

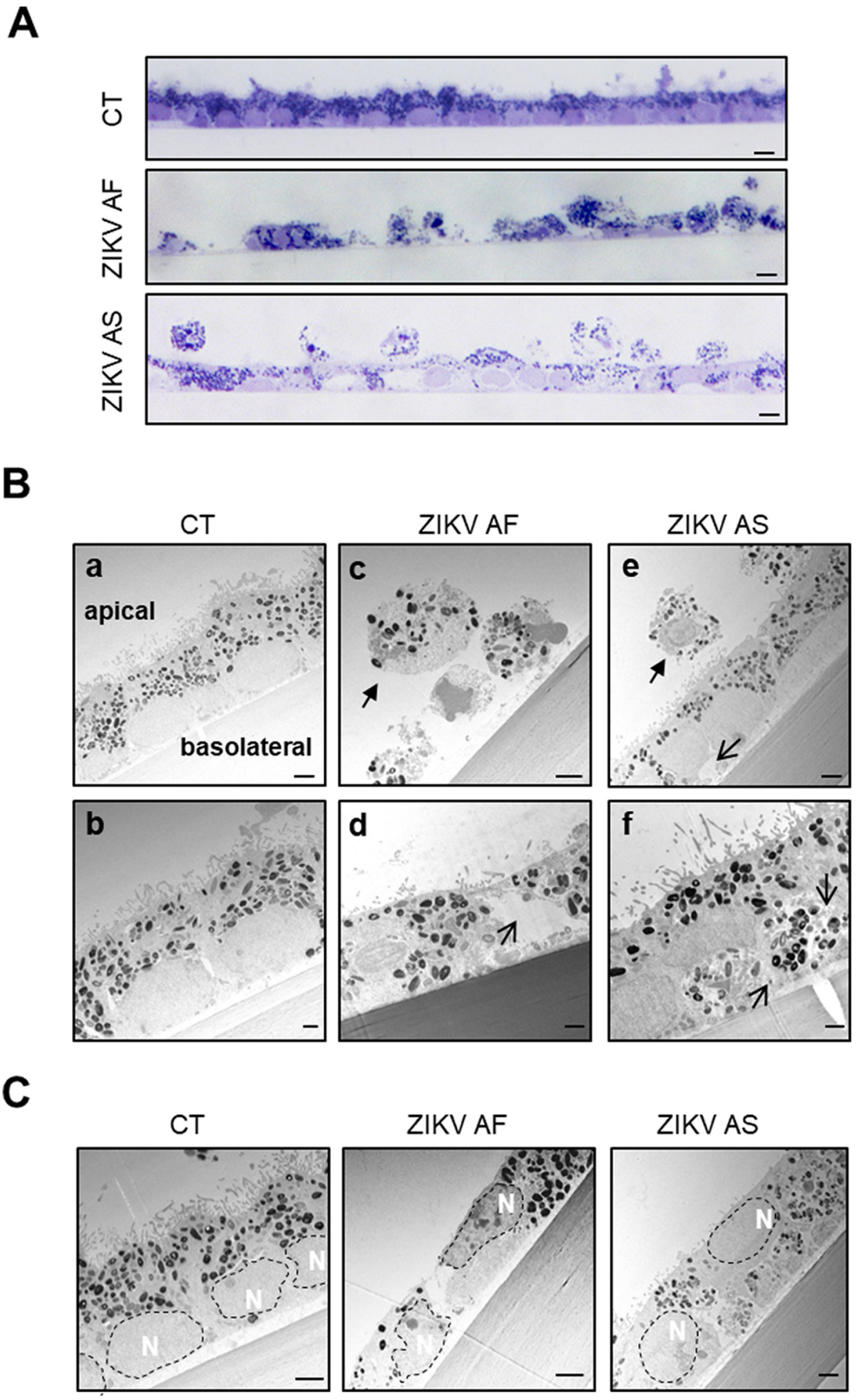

Fig. 2. ZIKV infection leads to RPE disorganization and nuclei mislocalization. Ultrastructural analyses of mock- or ZIKV-infected RPE grown on cell culture inserts at 10 dpi. (A) Semi-thin sections colored with toluidine blue show general RPE organization by light microscopy. Scale bars: 5 μm (B) Electron micrographs of mock- (a and b), ZIKV AF- (c and d) and ZIKV AS- (e and f) infected RPE. Plain arrows show rounded, detached cells and open arrows highlight vacuoles. Scale bars: a,c,e 2 μm, b,d,f 1 μm. (C) Analysis of electron micrographs of mock- and ZIKV-infected RPE shows changes in nuclei (dotted lines) location. Scale bars: 2 μm.

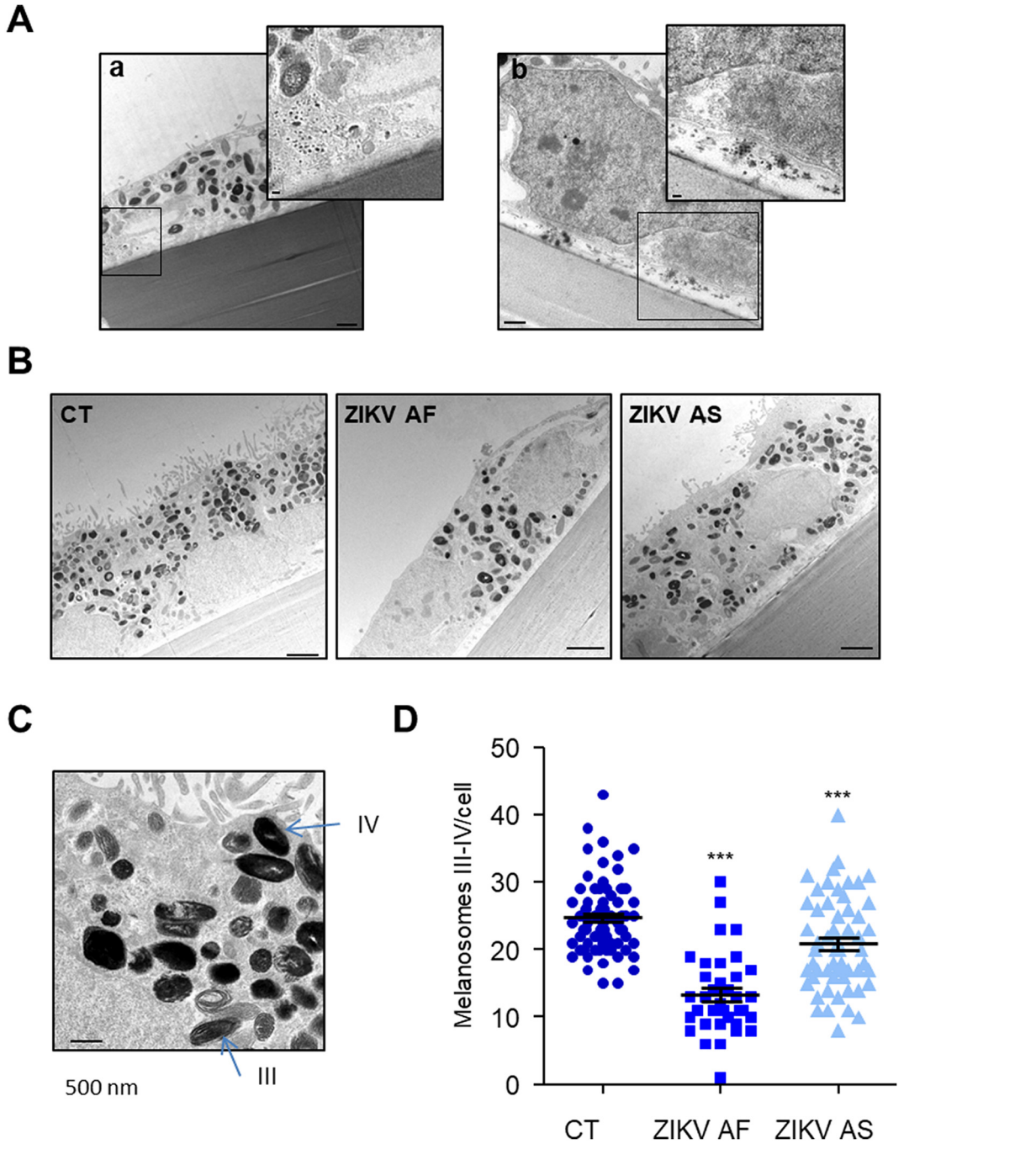

Fig. 3. ZIKV particles are present in the RPE and infection impacts the quantity of melanosomes. (A) Electron-dense particles with a size compatible to virions could be observed in ZIKV-infected cells (a and b). Inserts show higher magnification of black squares. Scale bars, a) 1 μm (insert 100 nm), b) 500 nm (insert 100 nm). (B) Mock- and ZIKV-infected cells display electron dense maturing and mature melanosomes. Scale bars 2 μm. (C) Different stages of melanosomes can be distinguished in CT RPE. Stages III and IV appear more electron dense due to the accumulation of melanin. Scale bars 500 nm. (D) Quantification of the number of melanosomes per cells in mock- and ZIKV-infected cells ($n = 37$ to 71 cells per condition). Results are expressed as means ± SEM and analyzed using an unpaired *t*-test, $^{***}p < .001$ compared to CT.

Representative images of electron micrographs are shown in Fig. 2B. Mock-infected epithelium, which displays a typical organization with tightly packed cells, basolateral nuclei, numerous melanosomes at different stages of biogenesis and apical microvillae (Fig. 2Bab), as we previously reported [31,43,49]. In ZIKV AF-infected epithelium, most of the cells appeared partially or completely detached (Fig. 2Bc), with a rounded or altered morphology compared to CT epithelia. When cells could be found attached to the culture support, they appeared elongated with numerous vacuoles and other architectural defects (Fig. 2Bd). Infection with ZIKV AS led to a less severe phenotype than ZIKV AF, as most of the cells were still attached to the support, even though a few rounded cells above the epithelial monolayer could be observed (Fig. 2Be). Some vacuoles and intracellular organelle disorganization could also be observed (Fig. 2Bf). This was seen in particular for the position of the nuclei, which, rather than the basolateral positioning as in CT epithelia, were sometimes closer to the apical surface in the epithelia infected with either strain (Fig. 2C). When individual cells where examined in more detail, optically dense particles with a size consistent to that of viruses could be observed either packed in intracellular structures (Fig. 3Ab), as was previously reported [52] or at the basolateral side of the epithelium (Fig. 3Ab). These observations are consistent with a potential viral release at this site, as we previously proposed [31] and confirmed in Fig. 1.

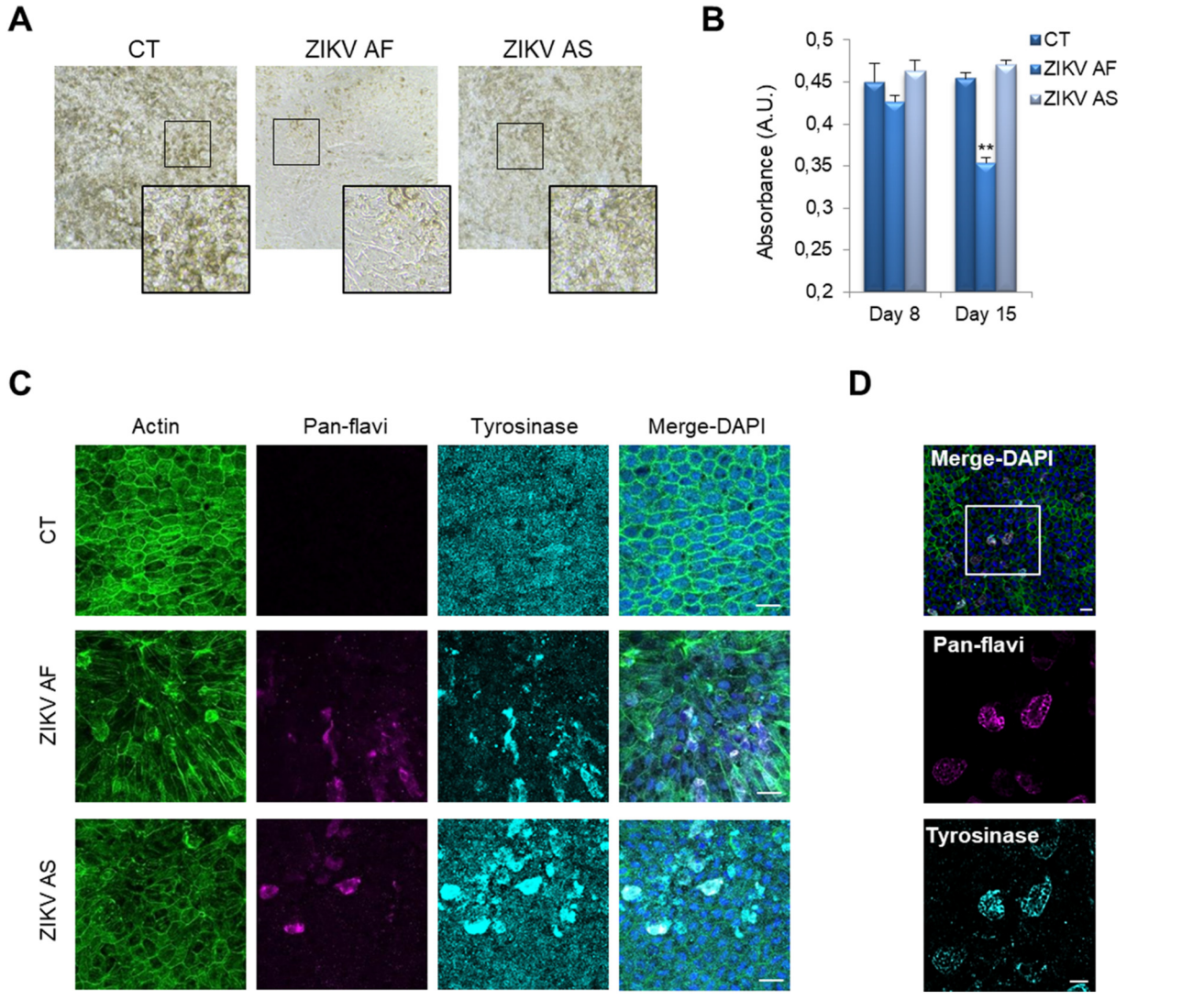

Fig. 4. ZIKV infection impairs melanosome biogenesis/homeostasis in RPE. (A) Light microscopy analysis of the pigmentation (brown) of mock- or ZIKV-infected RPE at 15 dpi. (B) Quantification of absorbance at 595 nm at various dpi in mock- and ZIKV-infected RPE. Results are expressed as means ± SEM ($n = 6–8$) and analyzed using an unpaired *t*-test, $^{**}p < .01$ compared to CT. (C) Indirect IF confocal studies at the same laser gain of mock- and ZIKV-infected RPE at 11 dpi to label actin (green), ZIKV (pan-flavi, magenta) and tyrosinase (cyan). Scale bars, 20 μm. (D) Imaging at lower gain shows colocalization between ZIKV (magenta) and tyrosinase (cyan) in ZIKV-infected RPE. Scale bars 20 μm, insert 10 μm.

Lastly, the pigmentation of the RPE cells is due to the presence of melanosomes, which can be seen to have an apical localization in the CT epithelia (Fig. 3B). Following infection with ZIKV AF and AS, the melanosomes appeared to be distributed more widely throughout the RPE and to be reduced in number as compared to CT. We therefore quantified late stages (III and IV) of melanosome biogenesis (Fig. 3C) and observed a significant reduction in melanosome number in ZIKV AF-infected cells, and to a lesser extent in ZIKV AS-infected RPE, as compared to CT, suggesting a potential impairment of organelle biogenesis or stability (Fig. 3D).

These ultrastructural analyzes confirmed the potent destabilization of the RPE epithelium by ZIKV infection. Organelle biogenesis/homeostasis may also be perturbed during the course of the infection as nuclei and melanosomes appeared affected.

3.3. ZIKV alters pigmentation in RPE cells

ZIKV infection can be associated with macular pigment mottling, indicating that RPE pigmentation is altered [23]. Moreover, our ultrastructural analyses suggested that melanosome biogenesis/homeostasis is affected by ZIKV AF and, to a lesser extent, by ZIKV AS. To test whether ZIKV could modify the pigment patterns of RPE, we used light microscopy to visualize/quantify pigmentation due to melanosomes. Fig. 4A shows strong pigmentation in mock-infected RPE with a typical polygonal organization at low magnification (Fig. 4A, left panel). In ZIKV AF-infected RPE, however, cells appeared elongated and less densely packed with melanosomes (*i.e.* clearer) (Fig. 4A, middle panel). This striking phenotype was not observed in ZIKV AS-infected RPE, although mild depigmentation seemed to have occurred (Fig. 4A, right panel). Quantification of absorbance by spectrophotometry confirmed the decrease in pigmentation in ZIKV AF-infected RPE at 15 dpi but did not show significant reduction in ZIKV AS-infected RPE, although some areas seemed visually lighter (Fig. 4B).

To monitor pigmentation and melanosome number/maturation using another approach, we performed indirect IF in mock- or ZIKV-infected RPE and labeled cells for actin, pan-flavivirus and tyrosinase, a marker of maturing melanosomes [53]. In mock-infected conditions, the tyrosinase staining showed a punctate labeling, consistent with intracellular organelles. In ZIKV-infected cells, this pattern was perturbed as strong tyrosinase accumulation appeared in RPE cells infected with both strains (Fig. 4C). Moreover, dotted labeling appeared in non-infected cells adjacent to in ZIKV AS-infected cells. This punctate pattern

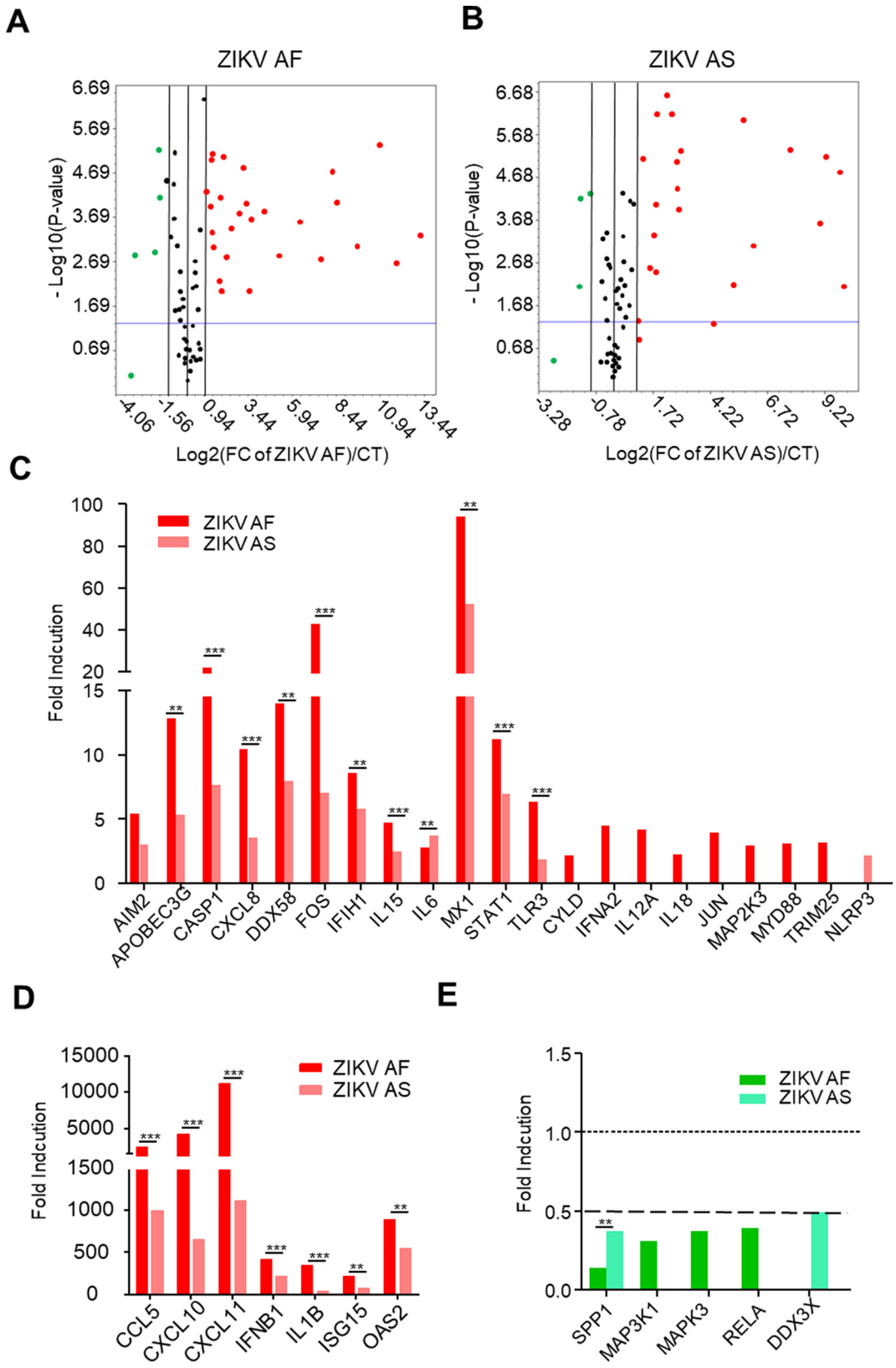

Fig. 5. Anti-viral response in ZIKV AF- or AS-infected RPE. mRNA from mock-, ZIKV AF- or ZIKV AS-infected RPE at 7 dpi were subjected to qRT-PCR analyses for the anti-viral response. Each point/histogram represents the mean of experimental triplicates. (A) and (B) Volcano plots of genes modulated upon ZIKV infection in RPE normalized to CT expression. Statistically significant changes in fold regulation appear in the top-right window (red; genes upregulated) and top-left window (green; genes downregulated). (C-E) Fold regulation of statistically significant genes modulated normalized to CT (upregulated (C and D) or downregulated (E)) in ZIKV AF- and ZIKV AS-infected RPE shown in (A) and (B). Results are expressed as means of the fold regulation and analyzed using an unpaired *t*-test, $^{*}p < .05$, $^{**}p < .01$ and $^{***}p < .001$ AF compared to AS (Supplemental Fig. 2B).

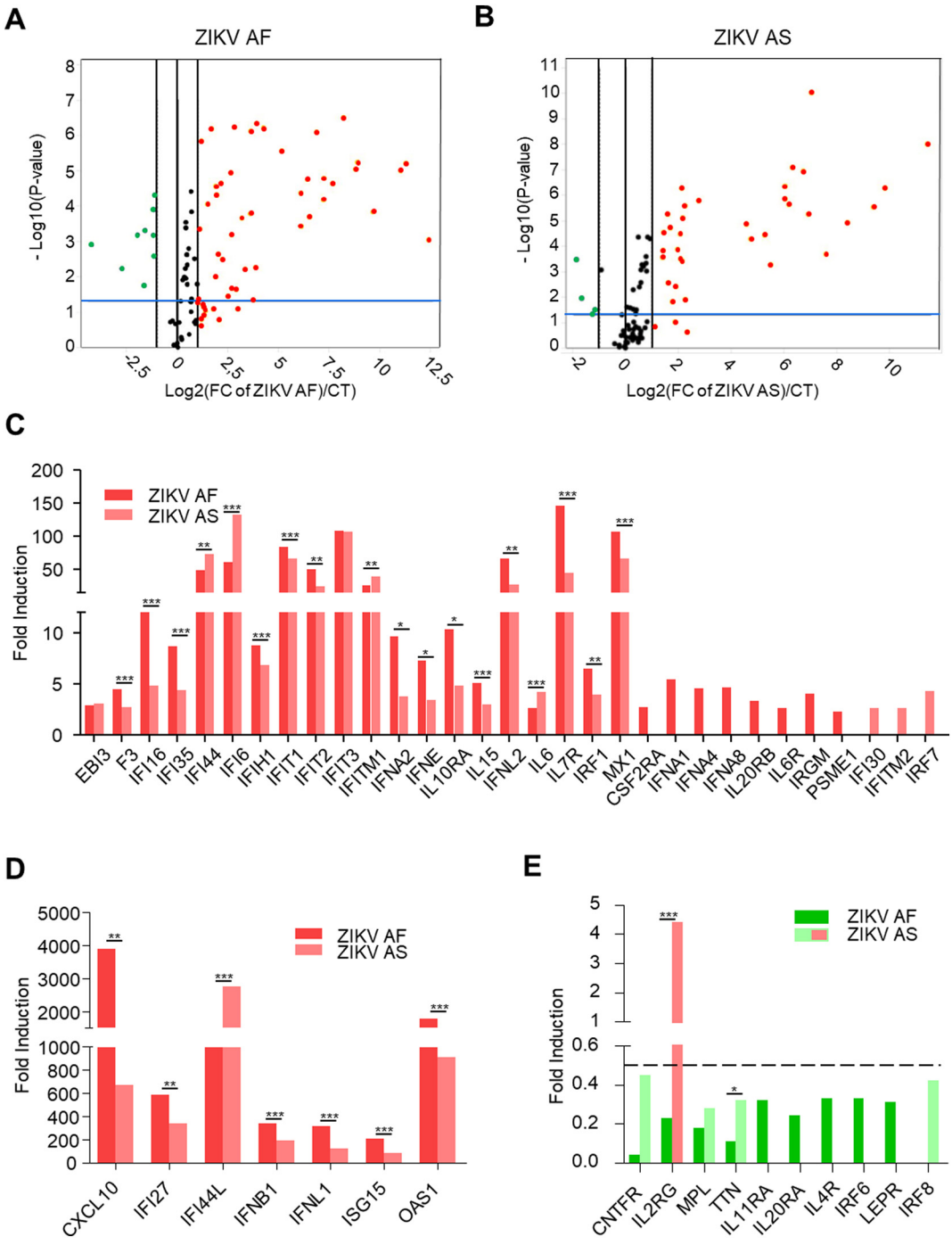

Fig. 6. Interferon responses in RPE infected by ZIKV AF or AS. qRT-PCR analysis using a specific interferon response PCR array of mRNA collected at 7 dpi from mock- ZIKV AF- (A) or ZIKV AS- (B) infected RPE. Each point/histogram represents the mean of experimental triplicates. (A) and (B) Volcano plots of genes modulated upon ZIKV infection in RPE normalized to CT expression. Statistically significant changes in fold regulation appear in the top-right window (red; genes upregulated) and top-left window (green; genes downregulated). (C–E) Fold regulation of statistically significant genes normalized to CT (upregulated (C and D) or downregulated (E)) in ZIKV AF- and ZIKV AS-infected RPE shown in (A) and (B). Results are expressed as means of the fold regulation and analyzed using an unpaired *t*-test, $^{*}p < .05$, $^{**}p < .01$ and $^{***}p < .001$ AF compared to AS (Supplemental Fig. 2D).

was, however, not seen in ZIKV AF-infected RPE cells, consistent with light microscopy observations (Fig. 4C). Interestingly, when ZIKV-infected cells were imaged at a lower gain (not to compare the punctate pattern), we could see a strong co-localization between virus labeling (the replication of which occurs in the endoplasmic reticulum) and the tyrosinase (Fig. 4D). This suggests that the trafficking of this key enzyme in melanosome biogenesis was impaired, which could in turn block the entire pathway.

This set of data suggests that melanosome biogenesis/homeostasis, and therefore pigmentation, is impaired by ZIKV infection in RPE cells.

3.4. ZIKV triggers strong anti-viral and multiple IFN type responses in RPE

Because African and Asian ZIKV strains showed different phenotypes in RPE cells, a trend that is currently emerging regarding the two ZIKV lineages [46], we next aimed to analyze and compare the anti-viral

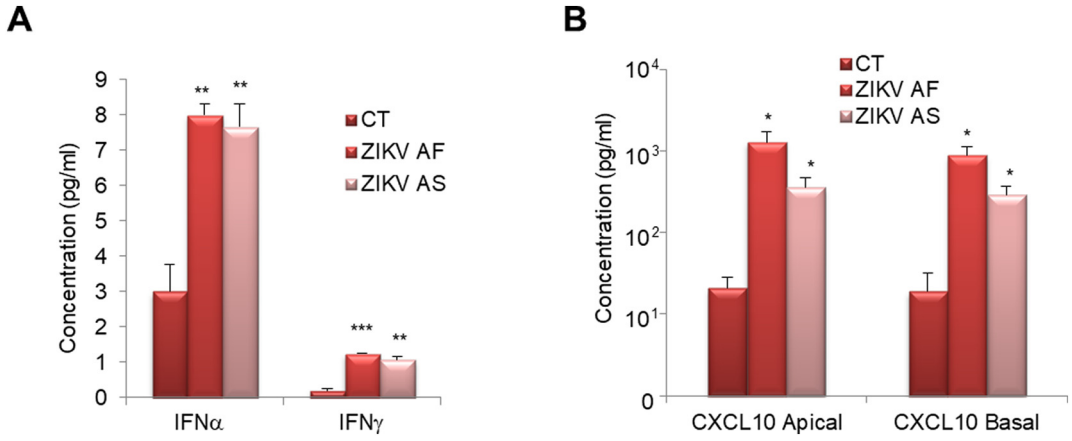

Fig. 7. Cytokine secretion is modulated in RPE upon ZIKV infection. Supernatants of mock- or ZIKV-infected RPE at 7 dpi were subjected to multiplex analyses. (A) Multiplex assay was performed to measure the concentration of IFNα, β γ and λ in supernatants. Only IFNα and γ were detected using this approach. Each histogram represents the mean + SEM (n = 3) (B). CXCL10 could be detected in the apical and basal compartments of RPE grown on cell culture inserts and collected at 7 dpi. Each histogram represents the mean + SEM from 3 independent experiments. Results were analyzed using an unpaired *t*-test, $^{*}p < .05$, $^{**}p < .01$, $^{***}p < .001$ compared to CT.

response in infected cells. To this end, we took advantage of a PCR array consisting of 84 genes involved in various pathways, including Toll-Like Receptor (TLR)-, Nod-Like Receptor-, RIGI-Like Receptor- and type-I-Interferon (IFN) Signaling [47]. Mock-, ZIKV AS- and ZIKV AF- (MOI 0.1) infected RPE cells were collected at 7 dpi, their RNA content extracted and cDNA was generated by reverse-transcription. Subsequent qPCR analyses were performed and showed potent gene induction and repression in ZIKV-infected cells (Fig. 5A and B). Twenty-seven genes were found to be upregulated (≥2 fold) in ZIKV AF-infected cells, whereas 20 genes were found to be upregulated (≥2 fold) in ZIKV AS-infected cells with a *p*-value ≤.05 (Fig. 5C and D, Supplemental Fig. 2). Genes involved in the type I IFN response, such as *INFB1*, and IFN responsive genes, such as *APOBEC3G*, *IL15*, *ISG15*, *MX1* and *TLR3*, were upregulated by both ZIKV AF and ZIKV AS. Similarly, TLR signaling genes (*e.g. MAP2K3*, *MYD88*, *JUN*), NOD signaling genes (*e.g. AIM2, NLRP3, OAS2, CASP1*) and RIG signaling genes (*e.g. DDX58/RIG-I*, *TRIM25*, *IFIH1/MDA5*) were upregulated upon infection. Many inflammatory cytokine and chemokine genes, including *IL12A, IL15, IL6, IL1B, CXCL10, CXCL8* and *CXCL11*, were found to be upregulated by both viral strains.

Moreover, 4 genes were found downregulated (≤2 fold) in ZIKV AF-infected cells (*MAP3K1, MAP3K, RELA, TKFC* and SPP1) and 2 genes (*DDX3X* and *SPP1*) were found downregulated (≤2 fold) in ZIKV AS-infected cells with a *p*-value ≤ .05 (Fig. 5E, Supplemental Fig. 2). Interestingly, in most cases, the two strains modulated differentially gene induction or repression. ZIKV AF had in the vast majority of cases a stronger effect (in induction and repression) than ZIKV AS, suggesting a more potent anti-viral response. In a few cases, only one strain was found to modulate gene expression, such as *INFA2*, *IL18, JUN, MYD88, TLR3* and *TRIM25* (ZIKV AF) and *NLRP3* and *DDX3X* (ZIKV AS).

Taken together, this set of data suggests that ZIKV infection in RPE elicits a strong anti-viral response, translated by possible cytokine secretion and associated immune-mediated responses. Similar to what was reported in other cellular systems, ZIKV AF triggered either stronger gene induction or stronger gene repression than ZIKV AS.

3.5. ZIKV modulates the three types of IFN responses following infection of RPE cells

The typical anti-viral response (whether for DNA or RNA viruses) involves mainly the type I IFNs, namely IFNα subtypes (α1–13), β, ε, κ and ω [54]. Type II IFN (γ) has limited direct anti-viral effects, but can promote adaptive and innate response through the modulation of immune cells. Type III IFNs (INFλ1–4) also elicit a strong anti-viral response but only for a specific subset of cells, for example mucosal surfaces and epithelia. Because ZIKV has been shown to trigger type II and III IFN signaling in other cellular systems [55,56], we next performed an in depth analysis of IFN signaling upon RPE infection by ZIKV AF and AS.

We used a PCR array designed to cover most IFNs, IFN receptors (IFNR), cytokines and other IFN responsive genes for the three types of IFN (84 genes, see Methods) in RPE at 7 dpi (MOI 0.1). A total of 49 genes were found significantly modulated (≥ or ≤ 2 fold, with a *p*-value ≤.05) (39 upregulated and 10 downregulated). ZIKV AF led to the upregulation of 35 genes whereas infection by ZIKV AS upregulated 31 genes (Fig. 6A and B, Supplemental Fig. 2). As expected from the previous results (Fig. 5), ZIKV infection modulated numerous genes involved in the type I IFN response including *IFNB1*, *INFA2*, *IFNE* (ZIKV AF and AS), *INFA1, INFA4, INFA8* (ZIKV AF) (Fig. 6C and D). Interestingly, type III IFN genes (*IFNL1* and *IFNL2*) were also found upregulated by both strains. However, *IFNG*, *INFGR1* and *INFGR2* were not modulated, suggesting that type II IFN signaling may not be targeted by ZIKV infection in this system. Some genes were found strongly (>200 fold) upregulated including *CXCL10* (as previously shown in Fig. 5D), *IFI27, IFI44L, IFNB1, IFNL1, ISG15* and *OAS1*. ZIKV strains also led to the downregulation of several genes including *CNTFR, MPL, IL2RG, TTN, IL11RA, IL20RA, IL4R, IRF6, LEPR* and *IRF8* (Fig. 6E).

Gene signatures modulated by ZIKV AF and ZIKV AS appeared rather complex as some genes were found more upregulated by ZIKV AF (*e.g. IFNE, CXCL10* and *IL7R*) or by ZIKV AS (*e.g. IFI44L* and *IFI6*), or just by one strain (*e.g. IFNA1* for ZIKV AF or *IRF7* for ZIKV AS). Similarly, some downregulated genes were only modulated by one of the ZIKV strains (*e.g. IL20RA* for ZIKV AF or *IRF8* for ZIKV AS). Surprisingly, one gene, *IL2RG*, was found modulated in the opposite way by both strains: ZIKV AF led to a downregulation, whereas ZIKV AS triggered an upregulation (Fig. 6E).

We next monitored the production of IFNs and selected cytokines in ZIKV-infected RPE. Supernatants from ZIKV AF- and ZIKV AS-infected RPE grown on cell culture inserts at 7 dpi were subjected to a multiplex assay aimed at measuring the concentration of some IFNs: IFNα, IFNβ, IFNλ and IFNγ (see Methods). Using this approach, we were able to detect the production of IFNα and IFNγ in ZIKV AF- and ZIKV AS- infected cells (Fig. 7A). Using a similar approach, we assayed the concentration of CXCL10 in both apical and basal compartment in mock- and ZIKV–infected RPE (Fig. 7B). CXCL10 was found potently produced in supernatants from both compartments by ZIKV AF- and ZIKV AS-infected cells, with a tendency for a higher induction observed for ZIKV AF (Fig. 7B).

These data suggest a complex interaction with the different types of IFN responses, with some unique gene modulations for a given strain. Type I and Type III IFN pathways were strongly modulated by both strains. Even though we were not able to detect a genetic modulation

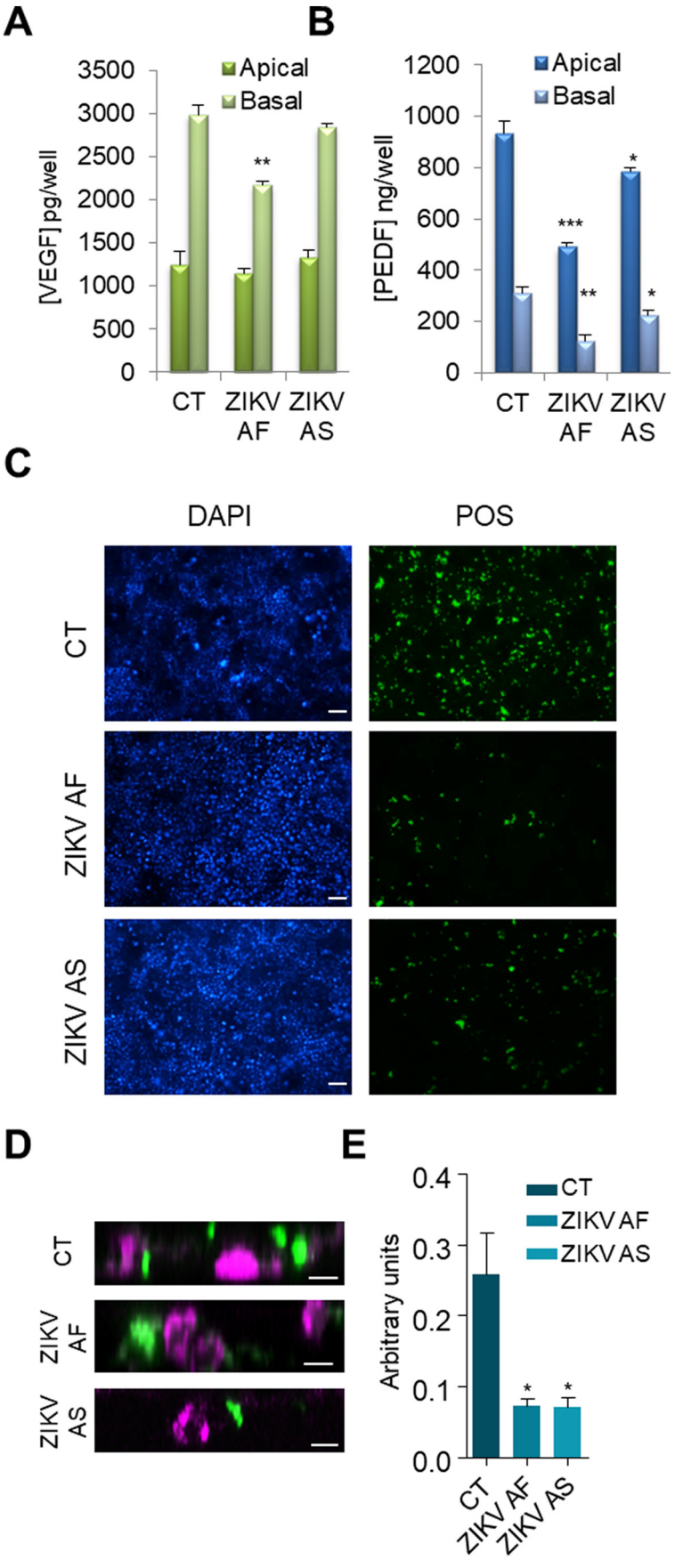
A
B
Apical
Basal
[VEGF] pg/well
3500
3000
2500
2000
1500
1000
500
0
**
CT
ZIKV AF
ZIKV AS
[PEDF] ng/well
1200
1000
800
600
400
200
0
***
**
*
C
DAPI
POS
CT
ZIKV AF
ZIKV AS
D
E
Arbitrary units
0.4
0.3
0.2
0.1
0.0
CT
ZIKV AF
ZIKV AS

of IFNγ, we could nonetheless observe a slight production by infected cells, suggesting that the three types of IFN response pathways were modulated by ZIKV infection in RPE. The monitoring of protein levels in supernatants could also suggest that despite gene activation, the secretion of some cytokines may be perturbed.

3.6. Secretion of survival factors and phagocytosis is impaired in ZIKV infected RPE

Membrane dynamics play a crucial role in RPE biology both for the production and secretion of essential factors for retinal homeostasis but also for the regulation of the visual cycle [57]. The impaired melanosome maturation and the reduction of some cytokines associated with ZIKV suggested that the secretory pathway could be impacted. Retinal homeostasis relies strongly on the production and activity of key survival factors, including vascular endothelial growth factor (VEGF, secreted primarily from the basal domain) and pigment epithelium-derived factor (PEDF, secreted primarily by the apical domain) [42,58]. To monitor whether secretion was affected in RPE cultured on porous cell inserts and infected by ZIKV, we performed ELISA assays to measure the concentration of VEGF and PEDF in the apical and basal compartments at 7 dpi (Fig. 8A and B). CT supernatants showed typical polarized secretion of VEGF (preferentially basal, Fig. 8A) and PEDF (preferentially apical, Fig. 8B). Although ZIKV AS did not significantly alter VEGF concentrations compared to CT, infection by ZIKV AF led to a significant decrease in the basal concentration of VEGF, whereas its apical quantity was not affected (Fig. 8A). By contrast, infection by the ZIKV strains led to a significant reduction in the concentration of PEDF in both compartments, with ZIKV AF having a stronger effect (Fig. 8B).

Because internalization of shed photoreceptor membrane disks is a key feature of RPE cells [36], we next measured whether photoreceptor outer segment (POS) phagocytosis was impaired upon ZIKV infection. Mock- or ZIKV-infected RPE at 7 dpi were incubated with fluorescently labeled bovine POS. Fig. 8C shows representative images of each condition, highlighting the cellular capture of labeled POS. A higher level of phagocytosis could be seen in the CT epithelia compared with the ZIKV-infected cells. *Z*-stack confocal imaging confirmed that POS were indeed internalized by ZIKV-infected RPE cells and were found often in close proximity (and at the same confocal planes) to the nucleus (Fig. 8D). Quantification of the mean fluorescence confirmed a significant decrease in POS uptake when cells were infected with either ZIKV AF or ZIKV AS (Fig. 8E).

These results suggest that ZIKV infection impairs the production/secretion of key survival factors and impacts the critical functions of the RPE, such as phagocytosis. Modulation of organelles and membrane dynamics during the course of infection may be responsible.

3.7. ZIKV AF efficiently targets the mouse eye

Finally, we aimed to compare the ocular invasion/replication between ZIKV AF and AS *in vivo*. To this end we used the *Ifnar*$^{-/-}$ mouse model [50], which is widely used to study flavivirus pathogenesis and for which ZIKV-dependent ocular pathology was described [35]. Mice were inoculated *via* the intraperitoneal route with PBS, ZIKV AF or ZIKV AS and euthanized at 7 dpi. Notably, ZIKV AF could be detected in the optic nerve (Fig. 9B top panel) and in the optic nerve head (Fig. 9A bottom panel), confirming as was previously suggested that axonal transport or cellular migration along the optic nerve could represent an entry for ZIKV into the retina [24]. Because our *in vitro* data suggest that ZIKV AF replicates more efficiently than ZIKV AS in the RPE, similarly to what we described in astrocytes and NSCs [47], we compared the amount of virus from the two strains found in the eye *in vivo*. Interestingly, RT-qPCR analysis after mRNA extraction from the eyes of PBS and ZIKV-inoculated animals showed that the ZIKV AF viral genome was found at a significant higher quantity (one log difference) than ZIKV AS (Fig. 9B), suggesting that the African strain is also likely to trigger ophthalmological pathologies.

Together, these observations are coherent with a more active virulence and ocular targeting for ZIKV AF and raise the question of the potential ophthalmological damages that could be associated with this lineage in patients.

4. Discussion

General ocular inflammation (uveitis) can be associated with infectious agents that reach the eye through the systemic route or the optic nerve. Typically, viral infection of the eye will lead to retinal impairment (defect in vasculature, cellular loss or outer blood retinal barrier disruption) [59]. The disruption of the blood-retinal barrier will in turn abolish the immune-privileged status of the eye and hence trigger infiltration and an immune response. An important component of the blood-retinal barrier is the RPE. Using a human iPSC-derived RPE model, we previously studied ZIKV infection of this tissue and showed that the Asian (AS) strain led to a breakdown in epithelium impermeability [31]. In this study, we compared ZIKV strains from African and Asian lineages and showed that both strains can efficiently infect the RPE and cause impairments in cellular architecture and organization. This was particularly notable for ZIKV AF, which led to a complete destabilization of the iPSC-derived RPE, while ZIKV AS, albeit leading to a loss of RPE impermeability, had milder effects. Consistently, ZIKV AF infection had a more pronounced effect on critical RPE functions, such as phagocytosis and growth factor secretion. Moreover, these impairments were mirrored by a strong anti-viral response and the modulation of multiple IFN responses, which differed in their quality and intensity between the two strains. Lastly, we showed that in the *Ifnar*$^{-/-}$ mouse model, ZIKV AF also targeted the eye efficiently and more robustly than ZIKV AS, suggesting that this strain may result in potentially stronger deleterious ophthalmological symptoms in humans.

The RPE is a target for numerous pathogens including viruses, such as Ebola [40], CMV [41,60], Varizella Zoster [61], and Influenza virus [62] or bacteria such as *Chlamydia trachomatis* [63]. In this context, the eye has been proposed to act as a reservoir, in particular for Ebola virus [18,40,64]. Several arboviruses have also been described to trigger ophthalmological damage [20,39]. Accumulating evidence in ZIKV-infected patients (from epidemic, Asian strains), as well as in cellular and animal models (mice and macaques) suggests that ZIKV displays a strong tropism for the eye, where it can cause pathologies including macular pigment mottling, chorioretinopathy and optic nerve atrophy ([17,30,35,65–67], 2017; [33]). The majority of clinical cases reporting ophthalmological anomalies upon ZIKV infection were in infants (suffering from microcephaly). Visual impairment is commonly found in these children months after birth, suggesting permanent damage [68]. Similarly, this was observed experimentally in congenital ZIKV-infected mice that reached adulthood and displayed motor and visual impairments [69]. However, ocular complications in adult humans also occur, which can be quite severe and lead to visual impairment [66,70]. Follow-up studies of these patients showed partial recovery but highlighted that permanent lesions due to prior ZIKV Asian strain

Fig. 8. Impairment of secretion of survival factors and phagocytosis of photoreceptor outer segments in RPE upon ZIKV infection. (A-B) ELISA analyses of VEGF (A) and PEDF (B) concentrations in the supernatants (from apical and basal compartments) of mock- or ZIKV-infected RPE grown on cell culture inserts at 7 dpi. Results are expressed as means ± SEM ($n = 3$) and analyzed using an unpaired *t*-test, $^{*}p < .05$, $^{**}p < .01$, $^{***}p < .001$ compared to CT. (C-E) Mock- or ZIKV-infected RPE grown on cell culture inserts at 7 dpi were incubated for 2.5 h with fluorescently-labeled POS (green), fixed, and imaged by epifluorescence (C) or confocal (D) microscopy; nuclei labeled with DAPI (blue) (D) Confocal imaging shows POS internalization (green) (in the same confocal plane as nuclei (false colored magenta). Scale bars (C) 50 μm, (D) 5 μm. (E) Quantification of the mean fluorescence from 6 random images of two independent experiments taken at a low magnification (10×) (ratio POS/DAPI).

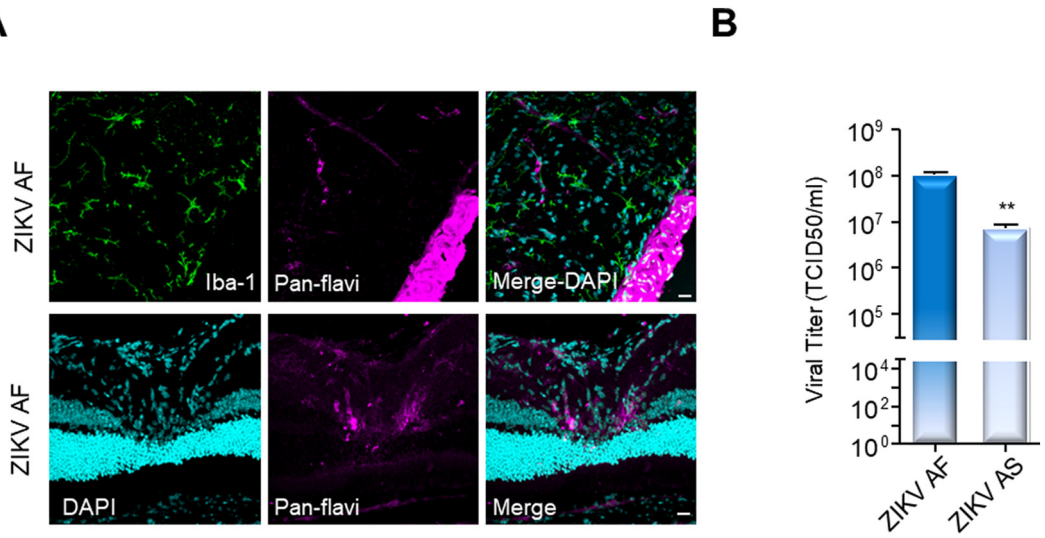

Fig. 9. ZIKV AF targets the mouse eye more efficiently than ZIKV AS after systemic infection. Mice were euthanized at 7 days post-intraperitoneal inoculation with 10^4 TCID50/ml of ZIKV AF or ZIKV AS. (A) 10 μm-thin retinal section of ZIKV AF-infected mouse eyes were stained for microglial cells (anti-Iba-1, green), ZIKV (pan-flavivirus, magenta) and nuclei (DAPI, cyan). ZIKV labeling (magenta) could be seen in the optic nerve (top panels) and in the optic chiasm (bottom panels). Representative images of 3 mice are shown. Scale bars (A) 10 μm. (B) ZIKV-specific RT-qPCR from mRNA of mock-, ZIKV AF- and AS-infected eyes. Results shown are mean from 3 animals + SEM and analyzed using an unpaired *t*-test, $^{**}p < .01$.

infection may be likely to persist [17,65]. In some adult patients, RPE disruption was observed [27], confirming the targeting of ZIKV to this tissue. Because ZIKV is found in conjunctival swabs from adult patients [12], lachrimal ZIKV-transmission has also been hypothesized, especially after one case report of a non-sexual transmission [6]. This was also demonstrated in mouse models [35], raising to the possibility that the eye is also acting as a reservoir for ZIKV. To date however, no clinical data have been reported regarding the potential ophthalmological impairments triggered by ZIKV African strains.

At the beginning of the South-American epidemic, a key question raised was whether the severe effects reported in some patients were due to specific evolution/mutation(s) of the Asian lineage that would cause more deleterious effects. It is now emerging that multiple mechanisms including changes in virus genome, vector transmission and host specification could be involved [71]. Accumulating evidence from our laboratories and others, are pointing however towards clear differences in virulence between the Asian and African strains ([46,72–74], 2016; [75,76]). Generally, ZIKV AF strains induce more potent anti-viral responses in various cellular systems [47,77,78] and now in RPE (this study). Moreover, interaction with cells of the immune system also differs between strains/lineages. For example, African strains were shown to replicate more efficiently and cause more cell death in dendritic cells (DCs) than Asian strains [79]. Our current data support these observations. Here we show that both ZIKV strains efficiently infect fully mature iPSC-derived human RPE at low MOI. Following ZIKV infection, we observed a more rapid drop in TER with the ZIKV AF (starting at 4 dpi), as compared to AS, which led to a loss of impermeability from 7 dpi onwards. By 11 dpi, impermeability was abolished for both strains. This was consistent with electron microscopy observations of RPE disorganization at 11 dpi with ZIKV AF and AS but which was more pronounced for the African strain.

Moreover, a key observation in our study was the difference in the anti-viral and interferon responses triggered by the two strains. This could be explained by the difference in replication kinetics of the two strains that we observed here, leading to a difference in viral copies/cell, which could trigger quantitatively and qualitatively different genetic responses. An alternative explanation would be that specific mutations that appeared in the ZIKV AS genome could be responsible for a different interaction/modulation of the immune response triggered against the virus. Generally, members of the *Flaviviridae* family, ZIKV included, can antagonize the type I IFN pathway, mainly *via* their well-conserved protein NS5 [56,80–83]. This ability to strongly inhibit type I IFN responses was proposed to favor a rather low-noise infection (*e.g.* in NSCs) that allowed Asian strains to persist in the host and cause long-term defects [84]. Interestingly, a mutation in ZIKV NS1 protein found in the epidemic Asian lineage (strain PRVABC-59) has been shown to better antagonize type I IFN response than a Cambodian (non-epidemic) strain [85]. However, this mutation is also found in African strains (Dakar-41,525) and cannot explain the tendency of ZIKV AF strains to better activate anti-viral and IFN responses as we and others observed [46,47].

Here we show that many genes involved in the classic anti-viral type I and III IFN responses, but also in type II IFN responses are differentially activated or repressed by the two ZIKV strains. It is noteworthy that gene modulation by both strains did not follow a simple pattern (*i.e.* one strain activated or repressed more than the other) but that a combination of effects on IFN responses was observed, as some genes were activated more by one of the two strains, or some were activated by one and not the other. This observation suggests that the difference in replication kinetics (*i.e.* the viral copy numbers) could not be the sole explanation for the generally "stronger" response triggered by ZIKV AF. This could be translated by a different effect on viral replication, persistence and cellular homeostasis, which could explain the general differences between African and Asian strains described *in vitro* and *in vivo*. For instance, ZIKV AS specifically induced *IF30* (an INFγ-responsive gene) whereas ZIKV AF specifically induced INFA genes such as *IFNA1*, *IFNA4*, *IFNA8*. This could reflect the general tendency of ZIKV Asian strains to either better inhibit or hide from anti-viral responses, which ultimately leads to some form of persistence, whereas ZIKV African strains appear more toxic for the cell/tissue/organism. Despite inducing a more potent anti-viral response, ZIKV AF was able to replicate more readily than ZIKV AS at early time points post-infection (up to 4 dpi), suggesting that the balance between how the virus escapes the IFN response and how the cell fights the infection is complex and most certainly involves a tug-of-war between viral and host proteins in the control of viral genome replication. These observations may also be consistent with a study showing that in monocytes, Asian strains modulate immunosuppressive genes (*e.g.* IL10, CD163, *etc.*), whereas African strains were associated more with the induction of inflammatory genes (*e.g.* CXCL10, IL18, *etc.*) [86].

One chemokine strongly upregulated by both lineages of ZIKV is CXCL10. CXCL10 is produced through the activation of IFN signaling,

and can be secreted by numerous cell type including leukocytes, monocytes endothelial and epithelial cells. It binds to the seven transmembrane-spanning G protein-coupled receptor CXCR3, which regulates chemotaxis of several immune cell types [87]. Beside its role in chemotaxis, CXCL10 was also shown to regulate apoptosis (*e.g.* during development, cancer and viral infections) and can activate numerous cells of the immune system including natural killer (NK) cells, T lymphocytes (Th1), macrophage and DCs [87]. Here, we detected a strong upregulation (ZIKV AF > ZIKV AS) both at the gene and protein levels in our cellular system. Interestingly, upregulated levels of CXCL10, together with IL10 and INFγ, were also detected in the eyes of mice infected systemically with ZIKV, [65]. This is also consistent with the higher production of some cytokines and markers of cell infiltration by African ZIKV strains *in vivo* [76]. In sera of ZIKV-infected patients, CXCL10 was found increased over 200 times compared to controls [88]. Because CXCL10 can be either beneficial or detrimental to viral infection [87], it is yet not clear what role this protein has in systemic or more localized ZIKV infection. Approaches with CXCL10 antagonists or blocking antibodies, as well as animal models deficient for this pathway may shed light on the role of this chemokine in ZIKV infection. Of note, CXCL10 has been implicated in various ocular disorders involving retinal degeneration [89–91].

Finally, RNA viruses are known to use and rearrange cellular membranes during their replication cycle [92]. Flavivirus replication mainly involves membranes originating from the ER as this cellular structure is diverted by the virus to allow compartmentalization and escape from host surveillance [93–95]. ZIKV has been shown to used ER-derived membranes during its replication, which in some cellular systems was followed by cell death [52,96,97]. We also found that in NSCs [47] and in the present study in RPE, ZIKV was located in the ER or ER-derived structures and that tyrosinase accumulated in these membranes. As the ER is a key component of the secretory pathway, which involve protein progression, membrane remodeling and organelle biogenesis [98], one can speculate that membrane dynamics is impacted in infected cells. In the RPE, even a low infectious dose may, with time, perturb critical functions of the RPE, such as phagocytosis and secretion. Along this line, the survival factors PEDF and VEGF, as well as their ratio and their polarized secretion, are essential for RPE integrity and function [58,99–101]. Here, we found both strains led to decrease of apical and basal PEDF secretion and that ZIKV AF, in addition, led to a significant decrease in basal VEGF secretion. This differential effect on the VEGF/PEDF ratio would trigger adverse effects on the RPE, and, *in vivo* on its neighboring tissues. In the case of ZIKV AF, these effects would be compounded by the lack of basal VEGF production.

Similarly, we found that ZIKV-infected cells, in particular ZIKV AF-infected RPE, showed less pigmentation, which was consistent with the quantification of fewer melanosomes, lysosome-related organelles that provide synthesis and storage of melanin [98]. ZIKV AS-infected RPE showed a slight but significant decrease in melanosome number, which was not mirrored by the less sensitive pigmentation quantification performed by light microscopy, suggesting a subtler impairment by the Asian strains. At this stage, we do not know whether ZIKV impairs the biogenesis, recycling/degradation or secretion of melanosomes. Clearly, the maturation/location of some key proteins involved in melanogenesis, such as tyrosinase [53], could be affected by ZIKV-induced ER impairment. Moreover, we found that both ZIKV strains impaired POS phagocytosis upon infection. Exocytosis and endocytosis are tightly coupled processes [98]. In RPE, phagocytosis of the photoreceptor outer segments is a key part of the visual system, which allows photoreceptor disk turnover and survival [36]. This phagocytic function also regulates RPE survival as it was shown that the internalized disk membranes provide lipids that allow synthesis of Neuroprotectin 1, which protects RPE form oxidative stress [102].

In conclusion, our results suggest that both *ex vivo* and *in vivo,* ZIKV AF targets more efficiently the retina. In iPSC-derived RPE, ZIKV AF infects/replicates more, which leads to a more potent destabilization of the RPE. The high production of pro-inflammatory cytokines (and potential immune cell recruitment) by ZIKV AF could translate into a more serious pathological effect in the eye than for ZIKV AS. In several cellular systems, in particular cells of the placenta or NSCs, the more potent virulence of ZIKV AF was proposed to potentially lead to pregnancy termination, rather than the developmental defects associated with the less virulent ZIKV AS ([74], 2017). Although we did not characterize the molecular mechanism(s) responsible for the difference in virulence between the two strains in the RPE, our data points towards a potential modulation of the host cell responses that varies depending on the ZIKV lineage used. Whether this is an early event (*e.g.* viral entry/trafficking), a later event in the replicative cycle (viral replication and interaction with host proteins), or a combination of several mechanisms is still unclear. One can also imagine that amplification of pathogenic cascades triggered by more virulent strains may also occur when a threshold in inflammatory or toxic molecules is produced upon infection. A strain able to better counteract these pathways (*i.e.* ZIKV AS) may trigger a longer lasting infection and associated impairments building overtime. Because the RPE is essential for retinal function by its role in the regulation of the visual cycle, as well as the integrity of the Bruch's membrane, the strong inflammatory response triggered by ZIKV is likely to be associated with a cascade of deleterious effects leading to impaired vision. Thus, because ZIKV AF is more virulent, in general and in the RPE in particular, one could expect that ophthalmological impairments associated with ZIKV infection would be more important with this lineage.

Acknowledgments

We thank Dr. Giles Uzé for the *Ifnar*$^{-/-}$ mouse model, Dr. Marie Pequignot (INM) for bovine POS isolation and assay, and members of our laboratory for technical help and support. We thank Chantal Cazevieille (Comet) for the processing of electron microscopy sections, Isabelle Sassetti (RHEM) for cryosections and the Montpellier RIO Imaging facility for confocal microscope imaging.

Funding resources

This work was funded by Retina France, REACTing and La Région Languedoc-Roussillon.

Conflict of interest

The authors declare no conflict of interest.

Author contributions

Conceived and designed the experiments YS, VK, SS; performed the experiments YS, NE, KD, MC, CD, KB, MT, ST, JB, GD, VF, SS; analyzed the data VK, SS; contributed reagents/materials/analysis tools ADL, ET, PDVP; contributed to the writing of the manuscript VK SS.

The following are the supplementary data related to this article.

References

[1] Dick GWA, Kitchen SF, Haddow AJ. Zika virus. I. Isolations and serological specificity. Trans R Soc Trop Med Hyg 1952;46:509–20.
[2] Musso D, Lanteri MC, Seligman S, et al. Emergence of Zika virus: where does it come from and where is it going to? Lancet Infect Dis 2017;17:255. https://doi.org/10.1016/S1473-3099(17)30070-1.
[3] Pettersson JHO, Eldholm V, Seligman SJ, Lundkvist, ??ke, Falconar AK, Gaunt MW, et al. How did zika virus emerge in the Pacific Islands and Latin America. MBio 2016;7:1–6. https://doi.org/10.1128/mBio.01239-16.
[4] Kelser EA. Meet dengue's cousin. Zika Microbes Infect 2016;18:163–6. https://doi.org/10.1016/j.micinf.2015.12.003.
[5] Moreira J, Peixoto TM, Siqueira AM, Lamas CC. Sexually acquired Zika virus: a systematic review. Clin Microbiol Infect 2017;23. https://doi.org/10.1016/j.cmi.2016.12.027.
[6] Swaminathan S, Schlaberg R, Lewis J, Hanson KE, Couturier MR. Fatal Zika virus infection with secondary nonsexual transmission. N Engl J Med 2016;375:1907–9. https://doi.org/10.1056/NEJMc1610613.

[7] Musso D, Nhan T, Robin E, Roche C, Bierlaire D, Zisou K, et al. Potential for Zika virus transmission through blood transfusion demonstrated during an outbreak in French Polynesia, November 2013 to February 2014. Eurosurveillance 2014;19:14–6.

[8] Musso D, Roche C, Robin E, Nhan T, Teissier A, Cao-Lormeau V-M. Potential sexual transmission of Zika virus. Emerg Infect Dis 2015;21:359–61. https://doi.org/10.3201/eid2102.141363.

[9] Nicastri E, Castilletti C, Balestra P, Galgani S, Ippolito G. Zika virus infection in the central nervous system and female genital tract. Emerg Infect Dis 2016;22:2228–30. https://doi.org/10.3201/eid2212.161280.

[10] Campos de MR, Cirne-Santos C, Meira GLS, Santos LLR, de Meneses MD, Friedrich J, et al. Prolonged detection of Zika virus RNA in urine samples during the ongoing Zika virus epidemic in Brazil. J Clin Virol 2016;77:69–70. https://doi.org/10.1016/j.jcv.2016.02.009.

[11] Blohm GM, Lednicky JA, Márquez M, White SK, Loeb JC, Pacheco CA, et al. Evidence for mother-to-child transmission of Zika virus through breast milk. Clin Infect Dis 2018;66:1120–1. https://doi.org/10.1093/cid/cix968.

[12] Sun J, Wu D, Zhong H, Guan D, Zhang H, Tan Q, et al. Presence of Zika virus in Conjunctival fluid. JAMA Ophthalmol 2016;134:1330. https://doi.org/10.1001/jamaophthalmol.2016.3417.

[13] Tan JJL, Balne PK, Leo Y-S, Tong L, Ng LFP, Agrawal R. Persistence of Zika virus in conjunctival fluid of convalescence patients. Sci Rep 2017;7:11194. https://doi.org/10.1038/s41598-017-09479-5.

[14] Kleber De Oliveira W, Cortez-Escalante J, De Oliveira WTGH, do Carmo GMI, Henriques CMP, Coelho GE, et al. Increase in reported prevalence of microcephaly in infants born to women living in areas with confirmed Zika virus transmission during the first trimester of pregnancy—Brazil, 2015. MMWR. Morb Mortal Wkly Rep 2016;65:242–7. https://doi.org/10.15585/mmwr.mm6509e2.

[15] Oliveira Melo AS, Malinger G, Ximenes R, Szejnfeld PO, Alves Sampaio S, Bispo De Filippis AM. Zika virus intrauterine infection causes fetal brain abnormality and microcephaly: tip of the iceberg? Ultrasound Obstet Gynecol 2016;47:6–7. https://doi.org/10.1002/uog.15831.

[16] Platt DJ, Miner JJ. Consequences of congenital Zika virus infection. Curr Opin Virol 2017;27:1–7. https://doi.org/10.1016/j.coviro.2017.09.005.

[17] Henry CR, Al-Attar L, Cruz-Chacón AM, Davis JL. Chorioretinal lesions presumed secondary to Zika virus infection in an immunocompromised adult. JAMA Ophthalmol 2017;135:386. https://doi.org/10.1001/jamaophthalmol.2017.0098.

[18] Kelly JD, Richardson ET, Barry M. Persistent Ebola virus in the eye. N Engl J Med 2015;373:1981–2. https://doi.org/10.1056/NEJMc1510459.

[19] Voigt V, Andoniou CE, Schuster IS, Oszmiana A, Ong ML, Fleming P, et al. Cytomegalovirus establishes a latent reservoir and triggers long-lasting inflammation in the eye. PLoS Pathog 2018;14:e1007040. https://doi.org/10.1371/journal.ppat.1007040.

[20] de Andrade GC, Ventura CV, Mello Filho PA, De A, Maia M, Vianello S, et al. Arboviruses and the eye. Int J Retin Vitr 2017;3:4. https://doi.org/10.1186/s40942-016-0057-4.

[21] Khairallah M, Ben Yahia S, Ladjimi A, Zeghidi H, Ben Romdhane F, Besbes L, et al. Chorioretinal involvement in patients with West Nile virus infection. Ophthalmology 2004;111:2065–70. https://doi.org/10.1016/j.ophtha.2004.03.032.

[22] Martínez-Pulgarín DF, Chowdhury FR, Villamil-Gomez WE, Rodriguez-Morales AJ, Blohm GM, Paniz-Mondolfi AE. Ophthalmologic aspects of chikungunya infection. Travel Med Infect Dis 2016. https://doi.org/10.1016/j.tmaid.2016.05.008.

[23] Agrawal R, Oo HH, Balne PK, Ng L, Tong L, Leo YS. Zika virus and eye. Ocul Immunol Inflamm 2017;00:1–6. https://doi.org/10.1080/09273948.2017.1294184.

[24] de Oliveira Dias JR, Ventura CV, de Paula Freitas B, Prazeres J, Ventura LO, Bravo-Filho V, et al. Zika and the Eye: pieces of a Puzzle. Prog Retin Eye Res 2018;66:85–106. https://doi.org/10.1016/j.preteyeres.2018.04.004.

[25] de Paula Freitas B, de Oliveira Dias JR, Prazeres J, Sacramento GA, Ko AI, Maia M, et al. Ocular findings in infants with microcephaly associated with presumed Zika virus congenital infection in Salvador, Brazil. JAMA Ophthalmol 2016;134:529. https://doi.org/10.1001/jamaophthalmol.2016.0267.

[26] Ventura CV, Maia M, Bravo-Filho V, Góis AL, Belfort R. Zika virus in Brazil and macular atrophy in a child with microcephaly. Lancet 2016;387:228. https://doi.org/10.1016/S0140-6736(16)00006-4.

[27] Kodati S, Palmore TN, Spellman FA, Cunningham D, Weistrop B, Sen HN. Bilateral posterior uveitis associated with Zika virus infection. Lancet 2016;6736:10–1. https://doi.org/10.1016/S0140-6736(16)32518-1.

[28] Parke DW, Almeida DRP, Albini TA, Ventura CV, Berrocal AM, Mittra RA. Serologically confirmed Zika-related unilateral acute maculopathy in an adult. Ophthalmology 2016;123:2432–3. https://doi.org/10.1016/J.OPHTHA.2016.06.039.

[29] Wong CW, Ng SR, Cheung CMG, Wong TY, Mathur R. ZIKA-RELATED MACULOPATHY. Retin Cases Brief Rep 2017;1. https://doi.org/10.1097/ICB.0000000000000552.

[30] Singh MS, Marquezan MC, Omiadze R, Reddy AK, Belfort R, May WN. Inner retinal vasculopathy in Zika virus disease. Am J Ophthalmol Case Rep 2018;10:6–7. https://doi.org/10.1016/j.ajoc.2018.01.023.

[31] Salinas S, Erkilic N, Damodar K, Molès J-P, Fournier-Wirth C, Van de Perre P, et al. Zika virus efficiently replicates in human retinal epithelium and disturbs its permeability. J Virol 2017;91. https://doi.org/10.1128/JVI.02144-16 e02144-16.

[32] Singh PK, Guest J, Kanwar M, Boss J, Gao N, Juzych MS, et al. Zika virus infects cells lining the blood-retinal barrier and causes chorioretinal atrophy in mouse eyes. JCI Insight 2017;2. https://doi.org/10.1172/jci.insight.92340DS1.

[33] Zhao Z, Yang M, Azar SR, Soong L, Weaver SC, Sun J, et al. Viral retinopathy in experimental models of Zika infection. Investig Opthalmology Vis Sci 2017;58:4075. https://doi.org/10.1167/iovs.17-22016.

[34] van den Pol AN, Mao G, Yang Y, Ornaghi S, Davis JN. Zika virus targeting in the developing brain. J Neurosci 2017;37:2161–75. https://doi.org/10.1523/JNEUROSCI.3124-16.2017.

[35] Miner JJ, Sene A, Richner JM, Ebel GD, Diamond MS, Apte RS, et al. Zika virus infection in mice causes Panuveitis with shedding of virus in tears. Cell Rep 2016;16:1–11. https://doi.org/10.1016/j.celrep.2016.08.079.

[36] Sparrrow JR, Hicks D, Hamel CP. The retinal pigment epithelium: normal functions and the related diseases. Curr Mol Med 2010;3.

[37] Detrick B, Hooks JJ. Immune regulation in the retina. Immunol Res 2010;47:153–61. https://doi.org/10.1007/s12026-009-8146-1.

[38] Roach T, Alcendor DJ. Zika virus infection of cellular components of the blood-retinal barriers: implications for viral associated congenital ocular disease. J Neuroinflammation 2017;14:43. https://doi.org/10.1186/s12974-017-0824-7.

[39] Cinatl J, Michaelis M, Fleckenstein C, Bauer G, Kabičková H, Scholz M, et al. West Nile virus infection induces interferon signalling in human retinal pigment epithelial cells. Invest Ophthalmol Vis Sci 2006;47:645–51. https://doi.org/10.1167/iovs.05-1022.

[40] Smith JR, Todd S, Ashander LM, Charitou T, Ma Y, Yeh S, et al. Retinal pigment epithelial cells are a potential reservoir for Ebola virus in the human eye. Transl Vis Sci Technol 2017;6:12. https://doi.org/10.1167/tvst.6.4.12.

[41] Tugizov S, Maidji E, Pereira L. Role of apical and basolateral membranes in replication of human cytomegalovirus in polarized retinal pigment epithelial cells. J Gen Virol 1996;77(Pt 1):61–74.

[42] Blenkinsop TA, Saini JS, Maminishkis A, Bharti K, Wan Q, Banzon T, et al. Human adult retinal pigment epithelial stem cell-derived RPE monolayers exhibit key physiological characteristics of native tissue. Invest Ophthalmol Vis Sci 2015;56:7085–99. https://doi.org/10.1167/iovs.14-16246.

[43] Cereso N, Pequignot MO, Robert L, Becker F, De Luca V, Nabholz N, et al. Proof of concept for AAV2/5-mediated gene therapy in iPSC-derived retinal pigment epithelium of a choroideremia patient. Mol Ther Methods Clin Dev 2014;1:14011. https://doi.org/10.1038/mtm.2014.11.

[44] Buchholz DE, Hikita ST, Rowland TJ, Friedrich AM, Hinman CR, Johnson LV, et al. Derivation of functional retinal pigmented epithelium from induced pluripotent stem cells. Stem Cells 2009;27:2427–34. https://doi.org/10.1002/stem.189.

[45] Hirami Y, Osakada F, Takahashi K, Okita K, Yamanaka S, Ikeda H, et al. Generation of retinal cells from mouse and human induced pluripotent stem cells. Neurosci Lett 2009;458:126–31. https://doi.org/10.1016/j.neulet.2009.04.035.

[46] Simonin Y, van Riel D, Van de Perre P, Rockx B, Salinas S. Differential virulence between Asian and African lineages of Zika virus. PLoS Negl Trop Dis 2017;11:e0005821. https://doi.org/10.1371/journal.pntd.0005821.

[47] Simonin Y, Loustalot F, Desmetz C, Foulongne V, Constant O, Fournier-Wirth C, et al. Zika virus strains potentially display different infectious profiles in human neural cells. EBioMedicine 2016;12:161–9. https://doi.org/10.1016/j.ebiom.2016.09.020.

[48] Kärber G. Beitrag zur kollektiven Behandlung pharmakologischer Reihenversuche. Arch Exp Pathol Pharmakol 1931;162:480–3. https://doi.org/10.1007/BF01863914.

[49] Torriano S, Erkilic N, Faugère V, Damodar K, Hamel CP, Roux A-F, et al. Pathogenicity of a novel missense variant associated with choroideremia and its impact on gene replacement therapy. Hum Mol Genet 2017;26:3573–84. https://doi.org/10.1093/hmg/ddx244.

[50] Hwang SY, Hertzog PJ, Holland KA, Sumarsono SH, Tymms MJ, Hamilton JA, et al. A null mutation in the gene encoding a type I interferon receptor component eliminates antiproliferative and antiviral responses to interferons alpha and beta and alters macrophage responses. Proc Natl Acad Sci U S A 1995;92:11284–8.

[51] Fronk A, Vargis E. Methods for culturing retinal pigment epithelial cells: a review of current protocols and future recommendations. J Tissue Eng 2016;7:1–23. https://doi.org/10.1177/2041731416650838.

[52] Monel B, Compton AA, Bruel T, Amraoui S, Burlaud-Gaillard J, Roy N, et al. Zika virus induces massive cytoplasmic vacuolization and paraptosis-like death in infected cells. EMBO J 2017:e201695597. https://doi.org/10.15252/embj.201695597.

[53] Mishima Y. Molecular and biological control of melanogenesis through tyrosinase genes and intrinsic and extrinsic regulatory factors. Pigment Cell Res 1994;7:376–87.

[54] Schneider WM, Chevillotte MD, Rice CM. Interferon-stimulated genes: a complex web of host defenses. Annu Rev Immunol 2014;32:513–45. https://doi.org/10.1146/annurev-immunol-032713-120231.

[55] Bayer A, Lennemann NJ, Ouyang Y, Bramley JC, Morosky S, Marques ETDA, et al. Type III interferons produced by human placental trophoblasts confer protection against Zika virus infection. Cell Host Microbe 2016;19:705–12. https://doi.org/10.1016/j.chom.2016.03.008.

[56] Chaudhary V, Yuen K-S, Chan JF-W, Chan C-P, Wang P-H, Cai J-P, et al. Selective activation of type II interferon signaling by Zika virus NS5. Protein J Virol 2017;91:1–17. https://doi.org/10.1128/JVI.00163-17.

[57] Sparrow JR, Hicks D, Hamel CP. The retinal pigment epithelium in health and disease. Curr Mol Med 2010;10:802–23.

[58] Kay P, Yang YC, Paraoan L. Directional protein secretion by the retinal pigment epithelium: roles in retinal health and the development of age-related macular degeneration. J Cell Mol Med 2013;17:833–43. https://doi.org/10.1111/jcmm.12070.

[59] Yoser SL, Forster DJ, Rao NA. Systemic viral infections and their retinal and choroidal manifestations. Surv Ophthalmol 1993;37:313–52. https://doi.org/10.1016/0039-6257(93)90064-E.

[60] Bodaghi B, Goureau O, Zipeto D, Laurent L, Virelizier JL, Michelson S. Role of IFN-gamma-induced indoleamine 2,3 dioxygenase and inducible nitric oxide synthase in the replication of human cytomegalovirus in retinal pigment epithelial cells. J Immunol 1999;162:957–64. https://doi.org/10.4049/jimmunol.169.10.5866.

[61] Graybill C, Claypool DJ, Brinton JT, Levin MJ, Lee KS. Cytokines produced in response to Varicella-Zoster virus infection of ARPE-19 cells stimulate lymphocyte chemotaxis. J Infect Dis 2017;216:1038–47. https://doi.org/10.1093/infdis/jix426.
[62] Michaelis M, Geiler J, Klassert D, Doerr HW, Cinatl J. Infection of human retinal pigment epithelial cells with influenza a viruses. Invest Ophthalmol Vis Sci 2009;50:5419–25. https://doi.org/10.1167/iovs.09-3752.
[63] Boiko E, Maltsev D, Savicheva A, Shalepo K, Khusnutdinova T, Pozniak A, et al. Infection of human retinal pigment epithelium with Chlamydia trachomatis. PLoS One 2015;10:e0141754. https://doi.org/10.1371/journal.pone.0141754.
[64] Varkey JB, Shantha JG, Crozier I, Kraft CS, Lyon GM, Mehta AK, et al. Persistence of Ebola virus in Ocular fluid during convalescence. N Engl J Med 2015;372:2423–7. https://doi.org/10.1056/NEJMoa1500306.
[65] Manangeeswaran M, Kielczewski JL, Sen HN, Xu BC, Ireland DDC, McWilliams IL, et al. ZIKA virus infection causes persistent chorioretinal lesions. Emerg Microbes Infect 2018;7:96. https://doi.org/10.1038/s41426-018-0096-z.
[66] Merle H, Donnio A, Jean-Charles A, Guyomarch J, Hage R, Najioullah F, et al. Ocular manifestations of emerging arboviruses: dengue fever, Chikungunya, Zika virus, West Nile virus, and yellow fever. J Fr Ophtalmol 2018;41:e235–43. https://doi.org/10.1016/j.jfo.2018.05.002.
[67] Mohr EL, Block LN, Newman CM, Stewart LM, Koenig M, Semler M, et al. Ocular and uteroplacental pathology in a macaque pregnancy with congenital Zika virus infection. PLoS One 2018;13:e0190617. https://doi.org/10.1371/journal.pone.0190617.
[68] Satterfield-Nash A, Kotzky K, Allen J, Bertolli J, Moore CA, Pereira IO, et al. Health and development at age 19–24 months of 19 children who were born with microcephaly and laboratory evidence of Congenital Zika virus infection during the 2015 Zika virus outbreak—Brazil, 2017. MMWR. Morb Mortal Wkly Rep 2017;66:1347–51. https://doi.org/10.15585/mmwr.mm6649a2.
[69] Cui L, Zou P, Chen E, Yao H, Zheng H, Wang Q, et al. Visual and motor deficits in grown-up mice with congenital Zika virus infection. EBioMedicine 2017;20:193–201. https://doi.org/10.1016/j.ebiom.2017.04.029.
[70] Zaidi MB, De Moraes CG, Petitto M, Yepez JB, Sakuntabhai A, Simon-Loriere E, et al. Non-congenital severe ocular complications of Zika virus infection. JMM Case Rep 2018;5. https://doi.org/10.1099/jmmcr.0.005152.
[71] Rossi SL, Ebel GD, Shan C, Shi PY, Vasilakis N. Did Zika virus mutate to cause severe outbreaks? Trends Microbiol 2018;xx:1–9. https://doi.org/10.1016/j.tim.2018.05.007.
[72] Anfasa F, Siegers JY, van der Kroeg M, Mumtaz N, Stalin Raj V, de Vrij FMS, et al. Phenotypic differences between Asian and African lineage Zika viruses in human neural progenitor cells. mSphere 2017;2. https://doi.org/10.1128/mSphere.00292-17 e00292-17.
[73] Dowall SD, Graham VA, Rayner E, Hunter L, Atkinson B, Pearson G, et al. Lineage-dependent differences in the disease progression of Zika virus infection in type-I interferon receptor knockout (A129) mice. PLoS Negl Trop Dis 2017;11:e0005704. https://doi.org/10.1371/journal.pntd.0005704.
[74] Sheridan MA, Balaraman V, Schust DJ, Ezashi T, Roberts RM, Franz AWE. African and Asian strains of Zika virus differ in their ability to infect and lyse primitive human placental trophoblast. PLoS One 2018;13:e0200086. https://doi.org/10.1371/journal.pone.0200086.
[75] Smith DR, Sprague TR, Hollidge BS, Valdez SM, Padilla SL, Bellanca SA, et al. African and Asian Zika virus isolates display phenotypic differences both in vitro and in vivo. Am J Trop Med Hyg 2018;98:432–44. https://doi.org/10.4269/ajtmh.17-0685.
[76] Tripathi S, Balasubramaniam VRMT, Brown JA, Mena I, Grant A, Bardina SV, et al. A novel Zika virus mouse model reveals strain specific differences in virus pathogenesis and host inflammatory immune responses. PLoS Pathog 2017;13:e1006258. https://doi.org/10.1371/journal.ppat.1006258.
[77] McGrath EL, Rossi SL, Gao J, Widen SG, Grant AC, Dunn TJ, et al. Differential responses of human fetal brain neural stem cells to Zika virus infection. Stem Cell Rep 2017;8:715–27. https://doi.org/10.1016/j.stemcr.2017.01.008.
[78] Zhang F, Hammack C, Ogden SC, Cheng Y, Lee EM, Wen Z, et al. Molecular signatures associated with ZIKV exposure in human cortical neural progenitors. Nucleic Acids Res 2016;44:8610–20. https://doi.org/10.1093/nar/gkw765.
[79] Bowen JR, Quicke KM, Maddur MS, Neal JTO, McDonald E, Fedorova NB, et al. Zika virus antagonizes type I interferon responses during infection of human dendritic cells. PLoS Pathog 2017:1–30. https://doi.org/10.1371/journal.ppat.1006164.
[80] Beaver JT, Lelutiu N, Habib R, Skountzou I. Evolution of two major Zika virus lineages: implications for pathology, immune response, and vaccine development. Front Immunol 2018;9. https://doi.org/10.3389/fimmu.2018.01640.
[81] Best SM. The many faces of the Flavivirus NS5 protein in antagonism of type I interferon signaling. J Virol 2017;91:1–14. https://doi.org/10.1128/JVI.01970-16.
[82] Grant A, Ponia SS, Tripathi S, Balasubramaniam V, Miorin L, Sourisseau M, et al. Zika virus targets human STAT2 to inhibit type I interferon signaling. Cell Host Microbe 2016:1–9. https://doi.org/10.1016/j.chom.2016.05.009.
[83] Kumar A, Hou S, Airo AM, Limonta D, Mancinelli V, Branton W, et al. Zika virus inhibits type-I interferon production and downstream signaling. EMBO Rep 2016;17:1766–75. https://doi.org/10.15252/embr.201642627.
[84] Sheridan MA, Yunusov D, Balaraman V, Alexenko AP, Yabe S, Verjovski-Almeida S, et al. Vulnerability of primitive human placental trophoblast to Zika virus. Proc Natl Acad Sci 2017:201616097. https://doi.org/10.1073/pnas.1616097114.
[85] Xia H, Luo H, Shan C, Muruato AE, Nunes BTD, Medeiros DBA, et al. An evolutionary NS1 mutation enhances Zika virus evasion of host interferon induction. Nat Commun 2018;9:414. https://doi.org/10.1038/s41467-017-02816-2.
[86] Foo S-S, Chen W, Chan Y, Bowman JW, Chang L-C, Choi Y, et al. Asian Zika virus strains target CD14+ blood monocytes and induce M2-skewed immunosuppression during pregnancy. Nat Microbiol 2017;2:1558–70. https://doi.org/10.1038/s41564-017-0016-3.
[87] Liu M, Guo S, Hibbert JM, Jain V, Singh N, Wilson NO, et al. CXCL10/IP-10 in infectious diseases pathogenesis and potential therapeutic implications. Cytokine Growth Factor Rev 2011;22:121–30. https://doi.org/10.1016/j.cytogfr.2011.06.001.
[88] Naveca FG, Pontes GS, Chang AYH, da Silva GAV, do Nascimento VA, Monteiro DC da S, et al. Analysis of the immunological biomarker profile during acute zika virus infection reveals the overexpression of CXCL10, a chemokine linked to neuronal damage. Mem Inst Oswaldo Cruz 2018;113:1–13. https://doi.org/10.1590/0074-02760170542.
[89] Liu F, Ding X, Yang Y, Li J, Tang M, Yuan M, et al. Aqueous humor cytokine profiling in patients with wet AMD. Mol Vis 2016;22:352–61.
[90] Nawaz MI, Van Raemdonck K, Mohammad G, Kangave D, Van Damme J, Abu El-Asrar AM, et al. Autocrine CCL2, CXCL4, CXCL9 and CXCL10 signal in retinal endothelial cells and are enhanced in diabetic retinopathy. Exp Eye Res 2013;109:67–76. https://doi.org/10.1016/j.exer.2013.01.008.
[91] Verhagen F, Kuiper J, Nierkens S, Imhof SM, Radstake T, de Boer J. Systemic inflammatory immune signatures in a patient with CRB1 linked retinal dystrophy. Expert Rev Clin Immunol 2016;12:1359–62. https://doi.org/10.1080/1744666X.2016.1241709.
[92] Inoue T, Tsai B. How viruses use the endoplasmic reticulum for entry, replication, and assembly. Cold Spring Harb Perspect Biol 2013;5:a013250. https://doi.org/10.1101/cshperspect.a013250.
[93] Blázquez AB, Escribano-Romero E, Merino-Ramos T, Saiz JC, Martín-Acebes MA. Stress responses in flavivirus-infected cells: activation of unfolded protein response and autophagy. Front Microbiol 2014;5:1–7. https://doi.org/10.3389/fmicb.2014.00266.
[94] Gillespie LK, Hoenen A, Morgan G, Mackenzie JM. The endoplasmic reticulum provides the membrane platform for biogenesis of the flavivirus replication complex. J Virol 2010;84:10438–47. https://doi.org/10.1128/JVI.00986-10.
[95] Mackenzie J. Wrapping things up about virus RNA replication. Traffic 2005;6:967–77. https://doi.org/10.1111/j.1600-0854.2005.00339.x.
[96] Gladwyn-Ng I, Cordón-Barris L, Alfano C, Creppe C, Couderc T, Morelli G, et al. Stress-induced unfolded protein response contributes to Zika virus–associated microcephaly. Nat Neurosci 2018;21:63–71. https://doi.org/10.1038/s41593-017-0038-4.
[97] Savidis G, McDougall WM, Meraner P, Perreira JM, Portmann JM, Trincucci G, et al. Identification of Zika virus and dengue virus dependency factors using functional genomics. Cell Rep 2016;16:232–46. https://doi.org/10.1016/j.celrep.2016.06.028.
[98] Wu L-G, Hamid E, Shin W, Chiang H-C. Exocytosis and endocytosis: modes, functions, and coupling mechanisms. Annu Rev Physiol 2014;76:301–31. https://doi.org/10.1146/annurev-physiol-021113-170305.
[99] Ablonczy Z, Prakasam A, Fant J, Fauq A, Crosson C, Sambamurti K. Pigment epithelium-derived factor maintains retinal pigment epithelium function by inhibiting vascular endothelial growth factor-R2 signaling through gamma-secretase. J Biol Chem 2009;284:30177–86. https://doi.org/10.1074/jbc.M109.032391.
[100] Farjood F, Vargis E. Physical disruption of cell-cell contact induces VEGF expression in RPE cells. Mol Vis 2017;23:431–46.
[101] Ford KM, Saint-Geniez M, Walshe T, Zahr A, D'Amore PA. Expression and role of VEGF in the adult retinal pigment epithelium. Investig Opthalmol Vis Sci 2011;52:9478. https://doi.org/10.1167/iovs.11-8353.
[102] Mukherjee PK, Marcheselli VL, Serhan CN, Bazan NG. Neuroprotectin D1: a docosahexaenoic acid-derived docosatriene protects human retinal pigment epithelial cells from oxidative stress. Proc Natl Acad Sci U S A 2004;101:8491–6. https://doi.org/10.1073/pnas.0402531101.